

An overview of the volatile systematics of the Lau Basin – Resolving the effects of source variation, magmatic degassing and crustal contamination

Doshik Hahm ^{a,1}, David R. Hilton ^{a,*}, Paterno R. Castillo ^a, James W. Hawkins ^a,
Barry B. Hanan ^b, Erik H. Hauri ^c

^a *Geosciences Research Division, Scripps Institution of Oceanography, UCSD, La Jolla, CA 92093-0244, USA*

^b *Department of Geological Sciences, San Diego State University, San Diego, CA 92182-1020, USA*

^c *Department of Terrestrial Magnetism, Carnegie Institution of Washington, NW Washington, DC 20015, USA*

Received 13 January 2011; accepted in revised form 7 February 2012; available online 18 February 2012

Abstract

The Lau Basin erupts lavas with a range of geochemical features reflecting a complex history of interaction involving different mantle sources. The Valu Fa Ridge (VFR) and Mangatolu Triple Junction (MTJ) region have lavas with arc-like characteristics, Niufo'ou Island (NV), Peggy Ridge and Central and Eastern Lau Spreading Centers (PR, CLSC and ELSC) erupt mid-ocean ridge basalt (MORB)-like volcanics, whereas the Rochambeau Bank (RB) has features akin to ocean island basalt (OIB). To characterize the volatile systematics of these various regions, we report a comprehensive study of 39 submarine lavas from these various eruptive centers encompassing analyses of the noble gases (He, Ne, and Ar) and carbon (CO₂) – both isotopes and abundances – together with other major volatile phases (H₂O, S, Cl, and F).

Helium isotope ratios of the NV, MTJ, CLSC, and ELSC are MORB-like for the most part except for differentiated lavas that tend to have lower, more radiogenic ³He/⁴He values. The RB has considerably higher ³He/⁴He ratios (up to 23 *R_A* in this work) which extend as far south as the PR. The influence of 'plume-like' sources in the RB is also apparent in Ne isotopes: RB samples follow a trend similar to Hawaiian basalts in 3-isotope neon space. However, RB lavas have lower ⁴⁰Ar/³⁶Ar (300–730) and higher [³⁶Ar] than CLSC and ELSC, suggesting greater air contamination. Elemental He/Ne ratios (³He/²²Ne_S and ⁴He/²¹Ne* where S = solar and * = nucleogenic) are high throughout the Lau Basin and identify the Lau mantle as one of only two high ³He/⁴He provinces worldwide with such an enrichment of He relative to Ne.

Magmatic CO₂ and δ¹³C fall in the range 7–350 ppm and –28‰ to –6‰, respectively. RB lavas have less [CO₂] and slightly lower δ¹³C than CLSC and ELSC. The lowest values are found among MTJ lavas. These lavas also have the highest [H₂O], [F], [Cl], and [S] whereas the PR, ELSC and CLSC have the lowest. RB has intermediate [H₂O]. We estimate primary [CO₂] in primary melts using [CO₂]-δ¹³C relationships, and find that RB lavas have higher [CO₂] (~935 ± 168 ppm) than ELSC/CLSC (638 ± 115 ppm). They also possess higher initial δ¹³C values, consistent with observations at other hotspot-related localities. However, there are no discernible differences in primary CO₂/Nb ratios between mantle sources characterized by high ³He/⁴He and MORB-like ratios. On the other hand, reconstructed values are considerably higher than that envisaged for depleted MORB mantle based on olivine-hosted melt inclusions.

© 2012 Elsevier Ltd. All rights reserved.

* Corresponding author.

E-mail address: drhilton@ucsd.edu (D.R. Hilton).

¹ Present address: Korea Polar Research Institute, Incheon 406-840, South Korea.

1. INTRODUCTION

The Lau Basin has seen concerted research activities in recent years, aimed at understanding its geological, tectonic, geochemical, and hydrothermal evolution (e.g., Baker et al., 2006; Jacobs et al., 2007; Pearce et al., 2007; Tian et al., 2008; Bezos et al., 2009; Escrig et al., 2009). This stems, in part, from its selection as an Integrated Study Site (ISS) as part of the Ridge 2000 Program of the US National Science Foundation. The focus of these studies has been the eastern basin – including the Eastern (ELSC) and Central (CLSC) Lau spreading centers – due to systematic variations in a number of parameters, e.g., spreading rate, distance from volcanic arc, etc., which form the basis of understanding ridge-related processes in a back-arc setting. However, other parts of the basin also present diverse and contrasting variations in petrology, morphology and crustal structure that can help define models linking the tectonic evolution of the Lau Basin with the underlying mantle source region. In this regard, reports of high $^3\text{He}/^4\text{He}$ ratios in the NW Lau (Rochambeau Bank region) have stimulated studies that integrate geochemical and seismic constraints on mantle flow fields (Turner and Hawkesworth, 1998; Smith et al., 2001).

In this study, we consider the helium isotope systematics of the Lau Basin and couple it with new data on the combined He–Ne–Ar–CO₂–H₂O–F–Cl–S characteristics of glasses from diverse areas of recent volcanic activity representing different tectonic settings and features within the basin. These settings include spreading ridges (Peggy Ridge – PR), Eastern and Central Lau spreading centers (ELSC and CLSC, respectively), seamounts (Rochambeau Bank, RB), volcanic islands (Niufo’ou Island – NV), and the Mangatolu Triple Junction (MTJ). We also report select data from the proximal Samoa hotspot. The primary aim of this study is to identify the major controls on the volatile systematics throughout the basin in order to reveal the extent of volatile heterogeneity in the underlying mantle source. In this way, we can tackle issues related to the geochemical evolution of the basin, the relative influence and extent of slab and hotspot inputs to extant mantle, and the potential role of pre-existing crust in areas of new and mature rifting. We utilize samples collected on three expeditions to the Lau Basin (see Section 2) thus gaining access to a broad coverage of various eruptive centers throughout the region. The same sample suite has already been utilized for complementary geochemical studies, e.g., major/trace elements and Sr–Nd isotopes, in the eastern Lau Basin (Tian et al., 2008).

2. GEOLOGICAL BACKGROUND AND SAMPLES

The Lau Basin is a trapezoidal area of seafloor that separates the 1100-km long Tonga Ridge to the east from the Lau Ridge (remnant arc) to the west (Fig. 1). The Tonga Ridge is a composite feature comprising an eastern belt of uplifted blocks of Tertiary platform carbonates, and a western belt of young active arc volcanoes, the Tofua Arc. The Lau Ridge was an active volcanic arc from at least the mid-Miocene (14 Ma) until the early Pliocene (2.5–1.5 Ma) (Gill, 1976; Cole et al., 1985; Woodhall, 1985).

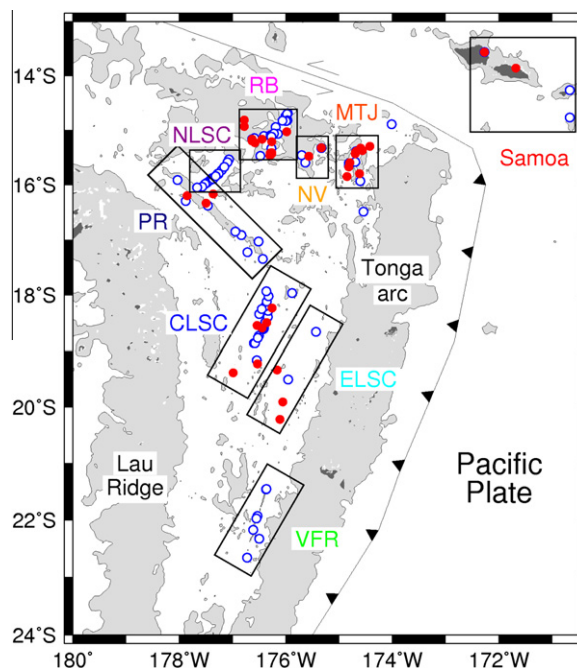


Fig. 1. Map of the Lau Basin. Based on geological feature and data availability, nine regions were defined: Valu Fa Ridge (VFR), Eastern Lau Spreading Center (ELSC), Central Lau Spreading Center (CLSC), Peggy Ridge (PR), Northern Lau Spreading Center (NLSC), Rochambeau Bank (RB), Niufo’ou Volcano (NV), Mangatolu Triple Junction (MTJ), and Samoa. All samples analyzed in this study (see Tables 1 and 2) are shown as red circles and other available $^3\text{He}/^4\text{He}$ data in the Lau Basin are shown as open circles (Poreda, 1985; Poreda and Craig, 1992; Poreda and Farley, 1992; Hilton et al., 1993; Honda et al., 1993; Bach and Niedermann, 1998; Lupton et al., 2009). Gray shade indicates areas shallower than 2000 m. (For interpretation of the references to color in this figure legend, the reader is referred to the web version of this article.)

Seafloor spreading in the Lau Basin was initiated less than 6 Ma ago and has propagated to the south as the basin opened (Parson and Hawkins, 1994). The back-arc basin has several constituent parts that include active ridges, older extended and rifted crust with basin-range structure, and sub-basins partly filled with lavas, seamounts, and uplifted blocks of older oceanic crust. Within the basin, the ELSC and CLSC constitute two series of overlapping ridge segments that each resulted from southward propagating rifts originating from the trace of a major intra-basin transform fault. The ELSC and CLSC rift tips are estimated to be propagating southward at ~ 120 mm/yr (Parson and Hawkins, 1994). The Valu Fa Ridge (VFR) lies at the propagating tip of the southern extension of the ELSC and constitutes one of the youngest locations of back-arc rifting in the basin. It extends for at least 165 km more or less parallel to the Tonga Ridge, and approaches to within ~ 40 km of the volcanic island of Ata in the Tofua Arc. In the northern basin, there is a short ridge segment north of PR called the Northern Lau Spreading Center (NLSC) and a three-limbed ridge system in the northeastern part of the basin called the Mangatolu Triple Junction (MTJ). Recently,

Lupton et al. (2009) reported the presence of the Rochambeau Rift (RR), which appears to be a right stepping extension of the NLSC to the northeast. Rochambeau Bank appears to occupy the junction between the NLSC and the RR. Region by region description of the petrology of the Lau Basin can be found in Appendix A.

In order to explore the various controls (degassing, contamination and mantle source variations) on the abundance and isotopic variation of volatiles in the Lau Basin, we analyzed 39 basaltic glasses for He and CO₂ (³He/⁴He, δ¹³C and abundances) and H₂O, F, S, and Cl (abundances only) (Tables 1 and 2). For these analyses, we used samples collected on two previous Scripps expeditions – Papatua (PPTU) Leg 4 (Hawkins, 1988) and Roundabout (RNDB) Leg 15 (Hawkins, 1989) – as well as seven new glasses collected during the Magellan (MGLN) Leg 8 expedition (October, 2006) which targeted seamounts from the Rochambeau Bank region. These seven samples and four others from RNDB-15 expedition were also analyzed for Ne and Ar isotopes (Table 3) in an effort to further constrain degassing processes and mantle source characteristics in the northern Lau Basin. Additionally, we collected two peridotite xenoliths from Samoa which were analyzed for He and, in one case, Ne isotopes.

All samples analyzed as part of this study are shown as solid circles in Fig. 1: locations of other samples from the literature, analyzed for helium isotopes and used for comparison, are shown as open circles (see figure caption for literature citations). We use geographic locations to discuss the major volatile features of the Lau Basin, and samples are sub-divided into nine regions: Valu Fa Ridge (VFR), Eastern Lau Spreading Center (ELSC), Central Lau Spreading Center (CLSC), Peggy Ridge (PR), Northern Lau Spreading Center (NLSC), Rochambeau Bank (RB), Niuafou Volcano (NV), Mangatolu Triple Junction (MTJ) and Samoa.

3. ANALYTICAL METHODS

Fresh glass from the outer rind of pillow lavas was hand-picked and ultrasonically cleaned in 50:50 mixture of acetone and methanol. The cleaned glasses were then examined under a microscope, and any samples with evidence of surficial alteration were discarded. The cleaned glass was analyzed for light noble gas (He, Ne and Ar) isotopes and abundances, carbon isotopes and CO₂ abundances, major volatile abundances (H₂O, CO₂, F, Cl, S) as well as major/trace element chemistry. The five analytical methods/facilities used for these procedures are briefly described as follows.

Helium isotopes were measured on a MAP 215-50 noble gas mass spectrometer following procedures and protocols described previously (e.g., Shaw et al., 2004; Macpherson et al., 2005). Vesicle-sited gases were liberated using an on-line crushing technique (Scarsi, 2000), and the released gases were purified using a combination of Ti and Zr–Al (SAES) getter pumps and charcoal/Al-frit traps held at liquid nitrogen temperature. The final separation of He from Ne was accomplished using a cryogenic-cooled charcoal-

lined trap using compressed helium as the coolant. Standard aliquots of air (1 R_A where $R_A = 1.4 \times 10^{-6}$) and Yellowstone Park He (16.45 R_A) were used to determine the abundance and isotopic composition of the samples. Typical crusher blanks were $\sim 6 \times 10^{-11}$ cm³ STP ⁴He.

Neon and Ar isotopes were measured with a VG5400 mass spectrometer equipped with a Faraday cup and Daly photo-multiplier detector (Craig et al., 1993). A custom-made piston-activated crusher was used to release gases under vacuum. The crusher consisted of a hardened stainless steel cylinder (2 cm inner diameter) and 5–6 disks of 0.5 cm thickness which fit inside the cylinder. Up to 3 g of glass chips were sandwiched between the disks and then squeezed by a metal rod driven by a hydraulic piston located outside the crusher. Pressures up to 5000 psi (345 bars) were used to pulverize the glasses. The released gas was purified using similar processing steps as described for the He measurement. Neon results were corrected for procedural blanks and contributions of doubly-charged ⁴⁰Ar and CO₂ to ²⁰Ne and ²²Ne, respectively, following Niedermann et al. (1993). Typical crusher blanks were 2×10^{-11} cm³ STP ²⁰Ne and 8×10^{-9} cm³ STP ⁴⁰Ar. These values were 1% or less of typical sample yields.

Carbon dioxide (CO₂) concentrations and isotopic ratios (¹³C/¹²C, reported relative to V-PDB) of the volcanic glasses were determined by the stepped heating method (Macpherson et al., 1999). Surface contaminants, introduced after/during eruption and/or during sample handling were removed by pre-cleaning with dichloromethane and low temperature combustion at 400 and 600 °C. Following combustion, samples were pyrolyzed in 100 °C increments from 700 to 1200 °C. At each step, the released CO₂ was purified with a variable temperature trap (Des Marais, 1978) and its abundance was measured with a Baratron capacitance gauge manometer in a calibrated volume of the preparation line. Following barometric measurement, CO₂ released during each pyrolysis step was collected in a glass tube for transfer to a VG PRISM mass spectrometer for δ¹³C analysis. For most glass samples, two distinct peaks in abundance were observed at 700–900 and 1000–1200 °C steps. This was taken as release of CO₂ from vesicles and glass matrix, respectively, and these compositions are reported separately in Table 2. Based upon replicate analyses of single samples, the reproducibility of CO₂ and δ¹³C in our measurement system is estimated at $\sim 2\%$ and $\pm 0.4\%$, respectively (Macpherson et al., 1999).

The abundances of H₂O, CO₂, F, S and Cl were determined by SIMS at the Department of Terrestrial Magnetism, Carnegie Institution of Washington (Hauri, 2002). The instrument used was a Cameca IMS 6f ion microprobe which measures volatile components sputtered from the glass matrix by a Cs⁺ primary beam. Consequently, reported results of volatile contents represent those dissolved in the glass matrix and not sited in vesicles.

All major and trace elements were analyzed by electron microprobe and inductively-coupled plasma mass spectrometric methods, respectively. The analytical methods used and precision and accuracy of the measurements are described in Tian et al. (2008).

Table 1
Sample locations and helium isotope results.

Sample	Latitude (S)	Longitude (W)	Depth (m)	He/He ^c (R_C/R_A)	He (10^{-9} cm ³ STP/g)	MgO* (wt%)	SiO ₂ * (wt%)
<i>Rochambeau Bank</i>							
MGLN8-D7-25	15°13'00"	176°16'00"	1716	15.3 ± 0.2	23.8 ± 0.1	5.56	50.83
MGLN8-D8-3	15°26'00"	176°16'00"	2255	22.6 ± 0.2	794 ± 3	6.15	50.32
MGLN8-D9-9	15°14'00"	176°35'00"	1745.5	12.1 ± 0.1	613 ± 3	8.71	49.02
MGLN8-D10-2	15°10'00"	176°27'00"	1742	10.0 ± 0.1	4590 ± 40	8.08	48.23
MGLN8-D11-8	14°56'00"	176°47'00"	1303.5	12.07 ± 0.09	412 ± 2	5.73	49.00
MGLN8-D12-1	14°49'00"	176°47'00"	1600.5	16.0 ± 0.1	36.7 ± 0.3	7.56	48.74
MGLN8-D14-2	15°02'00"	175°59'00"	1719.5	7.52 ± 0.06	3410 ± 10	13.78	–
PPTU4-24-2	15°25'20"	176°17'30"	2007.5	23.3 ± 0.2	230 ± 2	5.76	49.67
PPTU4-24-1 ^a	15°26'00"	176°16'00"	2007.5	22.1 ± 0.4	180 ± 5.4	5.94	50.22
PPTU4-24-3 ^a	15°25'00"	176°16'00"	2007.5	21.9 ± 0.4	180 ± 5.4	6.02	49.7
TWD-106-1 ^a	15°10'00"	176°38'00"	1325	11.0 ± 0.3	1130 ± 33.9	–	–
PPTU4-23-2 ^a	15°12'00"	176°38'00"	1748.5	14.1 ± 0.3	440 ± 13.2	6.63	48.88
PPTU4-23-3 ^a	15°12'00"	176°38'00"	1748.5	12.3 ± 0.2	1000 ± 30	7.41	48.65
<i>Mangatolu Triple Junction</i>							
RNDB15-19-1	15°40'40"	174°49'00"	2348.5	7.9 ± 0.1	120 ± 2.4	7.63	50.48
RNDB15-44-2	15°51'00"	174°51'00"	2564	7.5 ± 0.1	160 ± 3.2	8.16	49.58
RNDB15-47-8	15°18'00"	174°25'30"	1954.5	7.9 ± 0.1	120 ± 2.4	–	–
RNDB15-45-2(b.a.) ^b	15°36'00"	174°48'00"	2213	6.3 ± 0.1	3.6 ± 0.072	4.06	53.64
RNDB15-21-3(b.a.) ^b	15°22'30"	174°34'00"	2174	0.94 ± 0.01	2.7 ± 0.054	2.76	54.94
PPTU4-3-1(b.a.) ^b	15°23'30"	174°40'50"	2135	0.85 ± 0.01	1.8 ± 0.036	2.14	56.2
RNDB15-20-1(an.) ^b	15°26'00"	174°42'00"	2166.5	5.9 ± 0.1	75 ± 1.5	1.44	60.04
RNDB15-22-1(an.) ^b	15°20'00"	174°36'00"	2140	7.1 ± 0.1	1.1 ± 0.022	2.47	57.69
PPTU4-9-1(an.) ^b	15°24'00"	174°41'30"	2089	2.7 ± 0.1	2.5 ± 0.05	1.93	59.42
RNDB15-20-7(an.) ^b	15°26'00"	174°42'00"	2166.5	1.9 ± 0.1	3.2 ± 0.064	1.46	60.59
PPTU4-4-1	15°47'50"	174°37'00"	2055.5	8.17 ± 0.02	12 ± 0.24	6.64	49.72
<i>Peggy Ridge</i>							
PPTU4-21-2	16°12'00"	177°51'30"	2234.5	9.9 ± 0.2	58 ± 10	7.5	49.43
PPTU4-19-1=	16°10'00"	177°22'00"	2464	10.9 ± 0.2	3890 ± 117	9.51	49.17
PPTU4-20-5 ^a	16°20'00"	177°30'00"	1312	10.4 ± 0.2	2030 ± 61	8.98	48.19
<i>Niuafu'ou Volcano</i>							
PPTU4-6-3	15°19'30"	175°20'00"	1630.0	7.65 ± 0.02	1310 ± 30	8.11	48.54
PPTU4-11-1 ^a	15°29'00"	175°34'00"	1690	8.1 ± 0.2	370 ± 11	6.99	50.64
<i>Central Lau Spreading Center</i>							
RNDB15-35-1	18°35'32"	176°26'54"	2327.0	8.5 ± 0.1	4120 ± 82.4	–	–
RNDB-15-26-2	18°14'06"	176°15'30"	2390	8.6 ± 0.1	1530 ± 30.6	8.46	50.64
RNDB15-27-1	18°29'50"	176°21'30"	2321.5	8.3 ± 0.1	511 ± 10.22	7.48	50.91
PPTU4-30-1	18°33'00"	176°32'30"	2579	8.7 ± 0.1	535 ± 10.7	–	–
RNDB15-15-8	19°14'00"	176°32'00"	2380	8.5 ± 0.1	340 ± 6.8	5.23	50.69
RNDB15-11-8	19°23'30"	176°59'18"	2682	8.4 ± 0.1	405 ± 8.1	–	–
<i>Eastern Lau Spreading Center</i>							
RNDB15-31-1	19°20'30"	176°10'00"	3171.5	8.8 ± 0.1	464 ± 9.28	6.28	51.32
RNDB15-5-8	19°54'40"	176°03'36"	2482	9.5 ± 0.1	2610 ± 52.2	8.14	51.32
RNDB15-5-8d	19°54'40"	176°03'36"	2482	9.3 ± 0.1	3070 ± 61.4	8.14	51.68
RNDB15-7-5	20°13'30"	176°06'36"	2748	8.8 ± 0.1	1120 ± 22.4	5.93	–
<i>Samoa</i>							
Mt. Tagotala(ol) ^b	13°34'13"	172°16'24"	–	11.4 ± 0.1	50.9 ± 0.1	–	–
Laulii(ol) ^b	13°51'39"	171°40'50"	–	11.9 ± 0.1	34.98 ± 0.08	–	–

Not determined values are shown in dashes.

^a He results from Poreda and Craig (1992). The other volatiles in Tables 2 and 3 were obtained through this study.

^b b.a.: basaltic andesite; an.: andesite; ol: olivine. All others are basalts.

^c Measured ³He/⁴He ratios are corrected for the addition of atmospheric helium using measured He/Ne ratios (Hilton, 1996); R_C is the corrected ³He/⁴He value, R_A is the air ³He/⁴He value (1.4×10^{-6}).

* Major elements analyzed by electron microprobe (Tian et al., 2008).

Table 2
The results of carbon isotope and abundance of volatiles.

Sample	CO ₂ ^{v,a} (ppm)	δ ¹³ C ^{v,a} (‰)	CO ₂ ^{d,b} (ppm)	δ ¹³ C ^{d,b} (‰)	CO ₂ ^{m,c} (ppm)	CO ₂ ^{sims,d} (ppm)	H ₂ O (wt%)	F (ppm)	S (ppm)	Cl (ppm)	Nb* (ppm)
<i>Rocham beau Bank</i>											
MGLN8-D7-25	36	−13.6	51.7	−10.2	87.7	58	0.688	315.6	1424	930.7	8.9
MGLN8-D8-3	60.9	−10.9	74.1	−8.9	135	70	0.762	296.5	1337	664.2	7.95
MGLN8-D9-9	44.8	−7.8	72.8	−8.0	117.6	72	0.477	133.3	925	157.2	1.6
MGLN8-D10-2	84	−8.6	80.8	−8.5	164.8	57	0.576	147	1249	121.7	2.27
MGLN8-D11-8	18.7	−16.1	8.9	−13.4	27.6	9	0.814	479	1045	486	19.68
MGLN8-D12-1	12.8	−13.4	2.7	−	15.5	4	1.006	286	609	232	3.34
MGLN8-D14-2	68.8	−10.2	56.6	−10.7	125.4	68	0.445	190.2	976	72	2.65
PPTU4-24-2	49.9	−12.3	55	−10.2	105	78.1	0.86	364	1183	467	9.2
PPTU4-24-1	30.2	−11.1	78.4	−11.2	108.7	79.1	0.86	364	1194	477	14
PPTU4-24-3	26.7	−13.1	76.9	−9.4	103.6	79.8	0.83	354	1160	461	12
TWD-106-1	13.4	−12.4	56.9	−10.2	70.3	49.3	0.75	276	1054	442	−
PPTU4-23-2	34.2	−13.8	80.3	−9.3	114.6	75	0.56	276	1231	1034	1.33
PPTU4-23-3	42.1	−14.8	76.9	−10.7	119	78.9	0.58	251	1013	291	−
<i>Mangatolu Triple Junction</i>											
RNDB15-19-1	59.8	−13.6	72.2	−8.9	132	89.2	0.92	173	827	147	1.88
RNDB15-44-2	66	−8	55.1	−6.3	121	94.9	1.05	142	755	155	1.25
RNDB15-47-8	8.4	−12.2	18.8	−	27.2	19.1	1.54	288	731	527	4.1
RNDB15-45-2(b.a.)	8	−25.4	12.5	−25.5	20.5	4.3	1.77	446	710	709	4.17
RNDB15-21-3(b.a.)	3.2	−	4.5	−	7.6	5.6	1.81	707	837	1695	8.56
PPTU4-3-1(b.a.)	4.3	−	6.9	−	11.2	4	1.92	768	962	900	6.71
RNDB15-20-1(an.)	25.5	−20.8	93.1	−27.6	118.7	6.4	1.54	823	445	3771	12.51
RNDB15-22-1(an.)	38.2	−18	35	−17	73.2	30.2	1.52	634	917	1984	8.32
PPTU4-9-1(an.)	2.7	−	4.3	−	7	6	1.28	828	439	3355	11.45
RNDB15-20-7(an.)	5.2	−	6.8	−	11.9	4.1	1.46	893	356	2082	11.75
PPTU4-4-1	5.9	−14	13.4	−7.9	19.4	8.6	1.76	370	332	703	4.19
<i>Peggy Ridge</i>											
PPTU4-21-2	69.9	−12.4	94.1	−12	163.9	105.7	0.64	374	959	169	11.52
PPTU4-19-1	102.7	−8.8	165.3	−9	268	141.6	0.14	76	703	24	4.0
PPTU4-20-5	53.6	−9.5	111.5	−9.5	165.1	82	0.23	80	812	31	4.0
<i>Niufo'ou Volcano</i>											
PPTU4-6-3	66.3	−10.2	81.7	−8	148	114.8	0.36	147	1031	70	6.25
PPTU4-11-1	58.6	−12.5	84.5	−10.4	143.1	91.3	0.3	168	988	89	7.0
<i>Central Lau Spreading Center</i>											
RNDB15-35-1	203.7	−9.9	144.5	−8.5	348.2	190.9	0.32	165	1128	394	−
RNDB-15-26-2	23.1	−9	176.5	−9.3	199.7	126.1	0.12	73	740	65	0.77
RNDB15-27-1	200.7	−9.4	151	−9	351.7	141	0.25	107	813	81	1.38
PPTU4-30-1	47.8	−11.8	140.6	−10.1	188.4	163.6	0.22	119	1022	151	−
RNDB15-15-8	41.7	−17.1	132.4	−12.4	174	122.3	0.5	253	1502	540	−
RNDB15-11-8	21.8	−7.8	69.8	−6.7	91.6	63.1	1.15	123	884	162	−
<i>Eastern Lau Spreading Center</i>											
RNDB15-31-1	17	−12.6	231.8	−8.4	248.7	167.8	0.23	75	764	17	0.8
RNDB15-5-8	91.6	−8	171.9	−8.4	263.6	131.2	0.24	94	917	88	0.63
RNDB15-5-8d	99.2	−8.2	180.9	−8.2	280	131.2	0.24	94	917	88	0.63
RNDB15-7-5	69.7	−10.2	68.8	−7.7	138.5	88.8	0.95	191	1218	390	1.73

Values not determined are shown as dashes.

^a CO₂ abundance and isotopic ratio (relative to V-PDB) in vesicle phase.

^b CO₂ abundance and isotopic ratio (relative to V-PDB) dissolved in glass.

^c Magmatic CO₂ = sum of CO₂^v and CO₂^d.

^d CO₂ abundance measured with SIMS, representing CO₂ dissolved in glass.

* Nb contents (±5%).

4. RESULTS

4.1. Helium

In Table 1, we report new helium isotope and concentration results for 31 glasses from various parts of the Lau Basin as well as two xenoliths from Samoa. We also include He results for eight samples from Poreda and Craig (1992) as they were analyzed in this study for CO₂ and other volatiles (Sections 4.4–4.6). The new He results encompass all parts of the Lau Basin with the exception of VFR. However, given that He isotope variations along the VFR were reported previously (Hilton et al., 1993), there is now extensive coverage of He isotope variations throughout the Lau Basin (this work; Poreda, 1985; Poreda and Craig, 1992; Hilton et al., 1993; Honda et al., 1993b; Bach and Niedermann, 1998; Lupton et al., 2009), and the nearby Samoa hotspot (Poreda and Farley, 1992; Workman et al., 2004; Jackson et al., 2007).

The highest ³He/⁴He ratios for the entire Lau Basin are located in the RB region to the north of the PR. Poreda and Craig (1992) were the first to report the high values that characterized the region (up to 22.1 R_A for a seamount) although there was also marked variability in ratios with two other nearby localities recording ratios of 14.1 and 11.0 R_A (see Table 1). Poreda and Craig (1992) also reported values of 10.9 and 10.5 R_A along the NLSC, and Poreda (1985) reported two values of 9.5 R_A along the PR. Recently, Lupton et al. (2009) reported a range of ³He/⁴He values between 10.9 and 28.1 R_A for samples from north of the Rochambeau Bank, in the Rochambeau Rifts (RR), with the highest value found in the northernmost portion of the rifts (see Fig. 2). They also reported that high ³He/⁴He ratios (i.e., greater than the canonical MORB range of 8 ± 1 R_A; Graham, 2002) extend southwards throughout the NLSC to the PR (Fig. 2).

As part of this study, a sample was selected from the same dredge haul (PPTU-24) as the highest reported values of Poreda and Craig (1992): it gave a ³He/⁴He value of 23.3 R_A (Table 1) – in good agreement with previous values. Moreover, we observed a similar range in ³He/⁴He values (10–23 R_A, Table 1) as reported by Poreda and Craig (1992) for samples collected during our Magellan expedition to the RB in 2006. Significantly, our next highest value (22.6 R_A) was found within 3 km of the reported location of dredge PPTU-24, likely due to sampling of the same seamount. However, unlike the results of Lupton et al. (2009), who found ³He/⁴He as high as 28.1 R_A in the RR, ~100 km to the northeast of RB, none of our other samples from RB had ³He/⁴He ratios >20 R_A. Nonetheless, all our RB samples except one (MGLN8-D14-2 – located to the northeast) had values greater than the MORB range of 8 ± 1 R_A. Our new analysis of a basalt from the northwestern extreme of the PR gave a ³He/⁴He value of 9.9 R_A (Table 1).

In the northeastern part of the Lau Basin, the MTJ and NV are characterized by ³He/⁴He values equal to or below the MORB range. All samples on or close to NV have ³He/⁴He falling within the MORB range (Fig. 2; see also Lupton et al., 2009), but of the 11 MTJ samples collected on Papatau and Roundabout expeditions and analyzed in this study, a total of only five samples (four basalt and one basaltic andesite) have ³He/⁴He >7 R_A (Table 1). The other basaltic andesite or andesite samples have ³He/⁴He values between 0.85 and 6.3 R_A. Significantly, the differentiated samples tend to have lower He concentrations: in all cases but one (RNDB15-20-1), [He] falls below 10⁻⁸ cm³ STP/g (Table 1 and Fig. 3). The same characteristics of low ³He/⁴He and [He] were observed for differentiated samples from the VFR (Hilton et al., 1993), and were attributed to enhanced degassing coupled with addition of radiogenic He during magmatic differentiation and crustal interaction.

Table 3
The results of neon and argon isotope ratios.

Sample	²⁰ Ne/ ²² Ne	²¹ Ne/ ²² Ne	²⁰ Ne (10 ⁻⁹ cm ³ STP/g)	⁴⁰ Ar/ ³⁶ Ar	⁴⁰ Ar (10 ⁻⁹ cm ³ STP/g)	⁴ He/ ⁴⁰ Ar*
<i>Rochambeau Bank</i>						
MGLN8-D7-25	10.06 ± 0.10	0.0291 ± 0.0002	0.402 ± 0.006	298 ± 6	135.3 ± 0.2	20.9
MGLN8-D7-25b	9.64 ± 0.15	0.0288 ± 0.0004	0.21 ± 0.003	307 ± 6	79.9 ± 0.2	7.95
MGLN8-D8-3a	9.98 ± 0.18	0.0293 ± 0.0002	0.498 ± 0.008	339 ± 7	309 ± 1	20.0
MGLN8-D8-3b	10.29 ± 0.17	0.0306 ± 0.0004	0.1 ± 0.002	703 ± 14	83.8 ± 0.1	16.3
MGLN8-D8-3d	10.22 ± 0.12	0.0302 ± 0.0001	0.128 ± 0.001	537 ± 11	65.1 ± 0.1	27.1
MGLN8-D9-9	10.23 ± 0.21	0.0300 ± 0.0002	0.298 ± 0.005	541 ± 11	275.8 ± 0.7	4.89
MGLN8-D10-2	10.18 ± 0.23	0.0304 ± 0.0002	0.516 ± 0.013	728 ± 15	525 ± 1	14.7
MGLN8-D11-8	9.74 ± 0.03	0.02901 ± 0.0002	1.721 ± 0.011	302 ± 6	629 ± 2	30.4
MGLN8-D12-1	9.74 ± 0.16	0.0295 ± 0.0007	5.451 ± 0.1	294 ± 6	3141 ± 9	–
MGLN8-D14-2	10.32 ± 0.14	0.0314 ± 0.0005	0.121 ± 0.001	584 ± 12	118.4 ± 0.4	58.3
<i>Central Lau Spreading Center</i>						
RNDB15-35-1	10.21 ± 0.2	0.0312 ± 0.0002	0.125 ± 0.002	819 ± 16	136 ± 0.2	47.4
RNDB-15-26-2	10.05 ± 0.3	0.0295 ± 0.0005	1.35 ± 0.03	458 ± 9	583 ± 2	7.40
<i>Eastern Lau Spreading Center</i>						
RNDB15-5-8	10.08 ± 0.1	0.0299 ± 0.0002	0.46 ± 0.004	1125 ± 23	393.2 ± 0.9	10.6
RNDB15-7-5	9.83 ± 0.1	0.0294 ± 0.0002	3.15 ± 0.03	294 ± 6	1179 ± 4	–
<i>Samoa</i>						
Mt. Tagotala	10.62 ± 0.05	0.0347 ± 0.0003	0.48 ± 0.01	4139 ± 83	374 ± 22	0.147

Not determined values are shown in dashes.

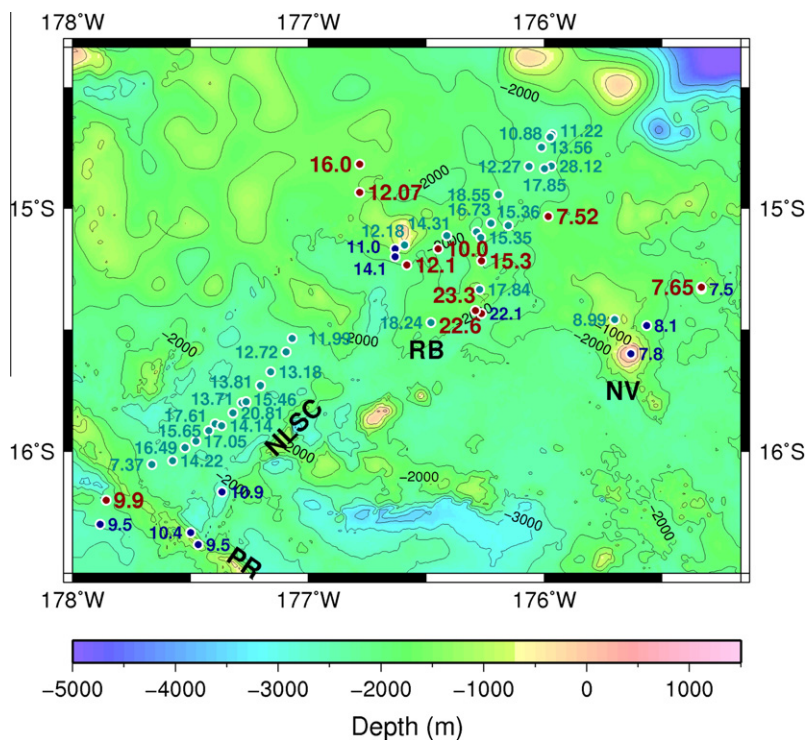


Fig. 2. $^3\text{He}/^4\text{He}$ (expressed relative to air value – R_A) in the samples from Rochambeau Bank and adjacent areas, superimposed on topography. The values in red were obtained in this work. The dark and light blues from Poreda and Craig (1992) and Lupton et al. (2009), respectively, are shown for comparison. (For interpretation of the references to color in this figure legend, the reader is referred to the web version of this article.)

The low He contents of the MTJ samples are in marked contrast to basalts from the CLSC and ELSC. These CLSC and ELSC samples are similar to MORB samples (e.g., Graham, 2002) in both He concentration ($\gg 0.3 \times 10^{-6} \text{ cm}^3 \text{ STP/g}$) and isotope composition – all samples have $^3\text{He}/^4\text{He}$ ratios $\sim 8 R_A$ with the exception of RNDB15-5-8 (ELSC) where duplicate analysis gave 9.3 and 9.5 R_A . Interestingly, Honda et al. (1993b) report another apparent outlier, in this case, for the CLSC: sample M2231-13 has a $^3\text{He}/^4\text{He}$ value of 11.2 R_A .

Finally, we report new analysis of peridotite xenoliths from a quarry on Savai'i Island and from a lava flow at Laulii, Upolu Island. The Savai'i sample was collected at the same place as 'Savi'i locality' of Poreda and Farley (1992) and gives $^3\text{He}/^4\text{He}$ of 11 R_A , consistent with their results. The Laulii sample gives 11.9 R_A , which is consistent with Upolu samples reported in Workman et al. (2004). However, the exact locations of their samples are not reported. In contrast, our $^3\text{He}/^4\text{He}$ results are lower than the results reported for Ofu Island located in the eastern province of the Samoan archipelago which fall in the range 19.5–33.8 R_A (Jackson et al., 2007).

4.2. Neon

Neon isotope analyses were performed on a subset of the samples analyzed for helium. The analyses were performed on seven glasses from the RB (Magellan expedition), two glasses each from the CLSC and ELSC and one xenolith

from Samoa (Table 3). The neon isotope results are shown on a three-neon-isotope diagram in Fig. 4. In addition to the RB samples (circles with dot; this study), we also plot basaltic glasses from the CLSC and ELSC (Honda et al., 1993b and this study) and olivines from Samoa (Poreda and Farley, 1992 and this study). For the stepped heating approach of Honda et al. (1993b), we include the 1000 °C fraction only as it shows the highest Ne isotope values. Non-atmospheric Ne was also released during the highest temperature step of Poreda and Farley (1992).

Two general features in the Lau Basin dataset are evident in Fig. 4. First, samples from the CLSC and ELSC fall close to the MORB-trend (Moreira et al., 1998), implying that these samples have coupled He and Ne systematics due to time integrated in-growth of radiogenic ^4He ($^4\text{He}^*$) and nucleogenic ^{21}Ne ($^{21}\text{Ne}^*$) (Honda et al., 1991, 1993a). In detail, however, the MORB-like CLSC samples fall on a slightly steeper slope than the MORB-trend defined by 'popping rock' (Moreira et al., 1998). This may reflect different primordial $^3\text{He}/^{22}\text{Ne}$ ratios in the mantle source in this region (Honda et al., 1993b) – see Section 5.5 for further discussion. Second, samples from the RB (this work) and Samoa (Poreda and Farley, 1992) lie on a trajectory which is steeper than MORB in Ne-isotope space: indeed, it is close to the trend defined by Loihi-Kilauea (Honda et al., 1991). The gradient of this trend is equivalent to a $^3\text{He}/^4\text{He}$ ratio of $\sim 24 R_A$ if He and Ne are coupled, according to the solar hypothesis of Honda et al. (1993b) which assumes $^3\text{He}/^{22}\text{Ne} = 3.3$. Interestingly, the deviations of

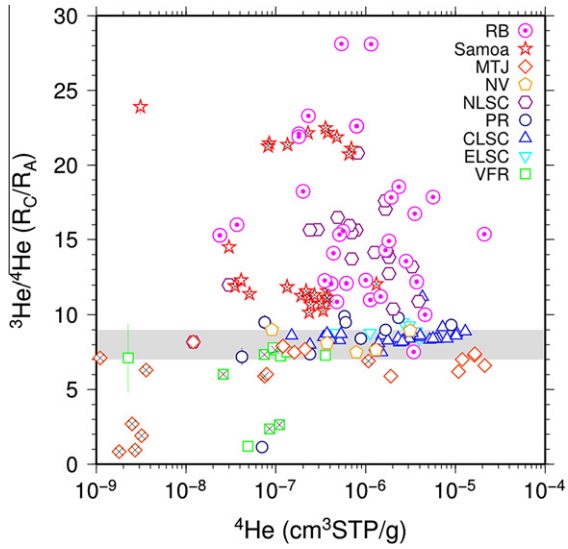


Fig. 3. Helium abundance and isotopic ratios of the samples from the Lau Basin and Samoa. Basaltic andesite or andesite samples from MTJ (diamond) and VFR (square) have x's. Stars with x's are olivine or pyroxene samples from Samoa. All other values are from basaltic glass. In addition to the data from this work, those from Poreda (1985), Poreda and Craig (1992), Poreda and Farley (1992), Honda et al. (1993b), Hilton et al. (1993), Bach and Niedermann (1998), and Lupton et al. (2009) are also included.

neon isotopic ratios of RB samples from the air value are generally less than those of Samoa and CLSC, indicating that these samples have a greater proportion of an atmospheric component. The atmospheric component can be introduced either during sample recovery from seafloor depths or during sample preparation in the laboratory through the development of micro-fractures in the samples allowing intrusion of atmospheric components (Ballentine

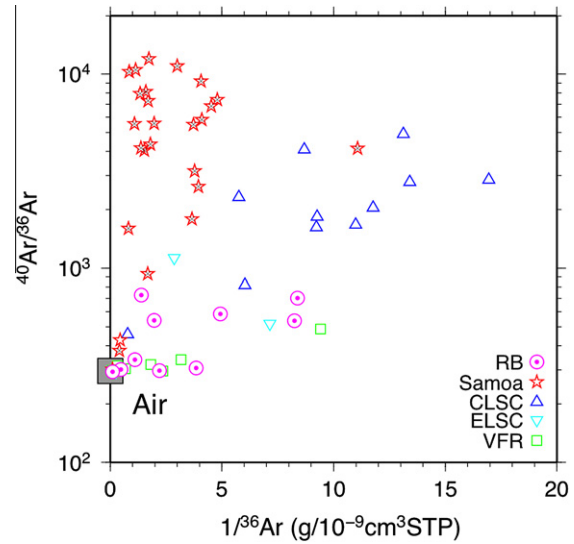


Fig. 5. Argon isotopic ratios in the Lau Basin samples. In addition to the present study, data from previous studies by Honda et al. (1993b), Hilton et al. (1993) and Poreda and Farley (1992) are also included.

and Barfod, 2000). Alternative possibilities for introducing air-like Ne include assimilation of seawater-derived components (Farley and Craig, 1994), and (mantle) recycling of subducted altered oceanic crust (Sarda, 2004).

We note also that the RB samples were erupted over a depth range between 1300 and 1700 m, which is far shallower than eruption depths of CLSC samples (2300–2600 m). Consequently, they have likely experienced more degassing than the CLSC samples, consistent with lower CO₂ contents than CLSC samples (Fig. 8), and are thus more susceptible to record the effects of addition of air-like Ne. Finally, we point out that one RB sample (MGLN8-

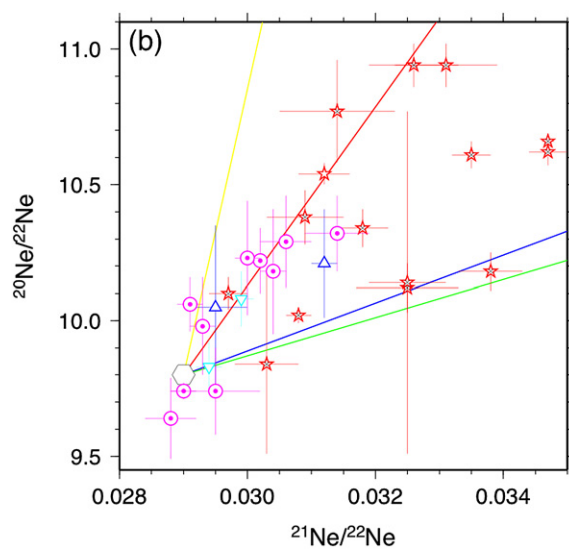
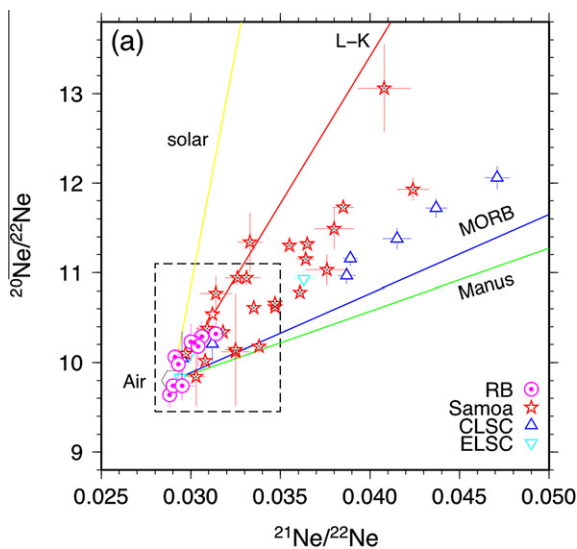


Fig. 4. Three neon isotope variations in the Lau Basin (this work; Poreda and Farley, 1992; Honda et al., 1993b). Symbols are the same as in Fig. 3. Hexagon stands for air component. (a) Ne isotope slopes of solar, Loihi–Kilauea (Honda et al., 1991), MORB (Sarda et al., 1988), and Manus Basin (Shaw et al., 2001) values are shown for comparison. (b) Blow-up of the dashed rectangular region in (a).

D14-2) seems to lie on a slightly shallower trajectory than the other RB samples: notably, it has a lower $^3\text{He}/^4\text{He}$ of $7.52 R_A$.

4.3. Argon

Argon isotope ratios of the 12 samples analyzed for Ne are given in Table 3 and displayed in Fig. 5. In addition to data obtained in this study, we include other Lau Basin Ar data for comparison (Poreda and Farley, 1992; Hilton et al., 1993; Honda et al., 1993b). The main feature of the Ar isotope systematics of the Lau samples is the general trend of high (non-atmospheric) $^{40}\text{Ar}/^{36}\text{Ar}$ values being associated with characteristic low $[\text{Ar}]$. The highest $^{40}\text{Ar}/^{36}\text{Ar}$ values (>1000) are found in the CLSC samples whereas RB, VFR and ELSC samples tend to have values <1000 . Higher ^{36}Ar concentrations are generally indicative of greater degrees of atmospheric contamination, and this is consistent with the lower $^{40}\text{Ar}/^{36}\text{Ar}$ values characteristic of these samples. The Samoa mantle xenoliths (Poreda and Farley, 1992) are different in this respect, having both high $^{40}\text{Ar}/^{36}\text{Ar}$ values and high ^{36}Ar contents. Such samples must have been insulated from air additions, which may well reflect the fact that fluids were captured and trapped by the olivine crystals at greater depths (in the mantle) prior to their transfer and eruption at the surface.

4.4. CO_2 and $\delta^{13}\text{C}$

We measured CO_2 concentrations and isotopic ratios using the stepped heating technique (Mattey et al., 1984; Macpherson et al., 1999). The great advantage of this approach is that it is possible to separate vesicle-sited CO_2 from that dissolved in the glass matrix and to obtain carbon isotopic ratios on both components.

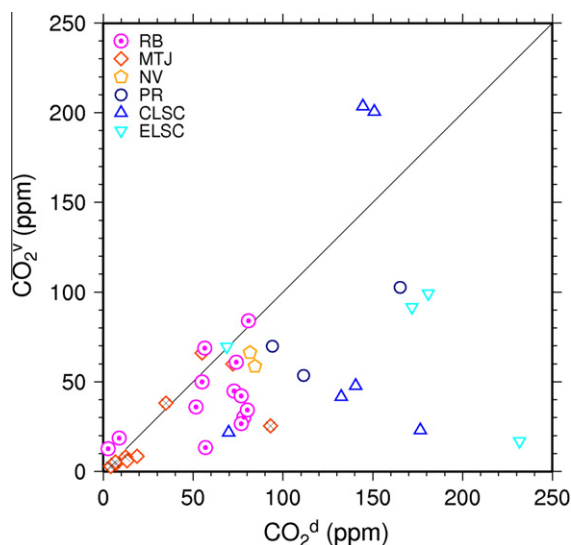


Fig. 6. Plot between CO_2 in vesicles (CO_2^v) and CO_2 dissolved in matrix (CO_2^d) measured by stepped heating method. Magmatic CO_2 (CO_2^m in Table 2) is dominated by CO_2^d for most of the samples.

The CO_2 concentrations of the Lau samples are illustrated in Fig. 6 which plots CO_2 in vesicles (CO_2^v) vs. CO_2 dissolved in the glass matrix (CO_2^d). Most of the samples fall below the 1:1 line, indicating the total magmatic CO_2^m ($\text{CO}_2^m = \text{CO}_2^v + \text{CO}_2^d$; Table 2) is generally dominated by CO_2 dissolved in the glass. The highest concentrations of CO_2 are found in samples from CLSC, ELSC and PR which have both CO_2^d and CO_2^m contents mostly $\gg 100$ ppm (Table 2). The highest concentration samples ($\text{CO}_2^m = 350$ ppm) are from the CLSC (RNDB15-35-1 and -27-1; Table 2). This observation may reflect the greater retention of vesicles in these samples as they have CO_2^d values similar to other CLSC samples. Both RB and NV samples have lower CO_2 contents – falling in the range of 50–90 ppm for CO_2^v and CO_2^d . Samples from MTJ have the lowest concentrations – all samples have CO_2^v and CO_2^d less than 100 ppm (Table 2) with only a few samples having a (combined) magmatic CO_2 (CO_2^m) greater than 100 ppm.

Carbon isotopic data from the stepped heating technique are summarized in Table 2. The samples from ELSC, CLSC, and RB have $\delta^{13}\text{C}^v$ and $\delta^{13}\text{C}^d$ in the range of -17.1‰ to -6.7‰ , roughly overlapping with each other. This range is similar to previous results for CLSC and ELSC (-16.4‰ to -8.8‰ ; Macpherson and Mattey, 1994). A few MTJ samples have $\delta^{13}\text{C}$ as low as -25‰ . Such low $\delta^{13}\text{C}$ values can result from fractionation associated with degassing (Macpherson and Mattey, 1994) and/or addition of slab-related organic C component (Shaw et al., 2004). One interesting observation is that, in most cases, $\delta^{13}\text{C}^d > \delta^{13}\text{C}^v$, i.e., Δ -values ($=\delta^{13}\text{C}^v - \delta^{13}\text{C}^d$) are negative. Because CO_2 vapor degassed from basalt is expected to be enriched in ^{13}C during equilibrium degassing (Javoy et al., 1978; Mattey, 1991), Δ is expected to be positive. Thus, the dominance of negative values in our samples indicates that vesicle gas CO_2 is not in equilibrium with

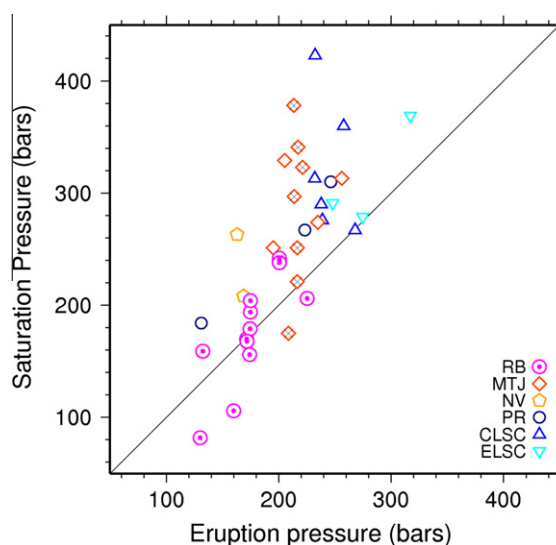


Fig. 7. Plot between saturation and eruption pressures. The saturation pressures are calculated using VolatileCalc 1.1 (Newman and Lowenstern, 2002) with CO_2^{sim} . Most of the samples fall above 1:1 line, indicating over-saturation with CO_2 .

dissolved CO_2 in the same sample, and could have been derived from degassing from magma elsewhere in the system (see discussion in Shaw et al., 2004). Alternatively, Aubaud et al. (2004) argued that isotope fractionation could produce Δ -values as low as -8.2% in pure kinetic (diffusive) degassing assuming that carbonate is the diffusing species. However, this mechanism appears to apply to samples which are extremely supersaturated ($\times 3$) – this is not the case for the majority of samples in this study (Fig. 7).

In addition to the stepped heating results, we obtained dissolved CO_2 contents using SIMS ($\text{CO}_2^{\text{SIMS}}$ in Table 2). There is excellent agreement between CO_2 contents between SIMS ($\text{CO}_2^{\text{SIMS}}$) and stepped heating (CO_2^{d}) techniques, as found previously between FTIR and stepped heating technique (Macpherson et al., 1999). We use the $\text{CO}_2^{\text{SIMS}}$ (or CO_2^{d}), together with H_2O , to determine whether samples are close to equilibrium solubility for their depths of eruption. In Fig. 7, we plot the saturation vapor pressure of each sample – which is based on the H_2O – CO_2 solubility model of Dixon et al. (1995) and calculated using VolatileCalc 1.1 (Newman and Lowenstern, 2002) – against confining pressure at the depth of eruption. Most of the Lau samples fall above the 1:1 line, indicating they are oversaturated with CO_2 . Such an observation is consistent with rapid eruption whereby degassing is inhibited (Dixon et al., 1988). However, the RB samples are generally at CO_2 equilibrium for their depth of eruption implying relatively slow magma ascent and eruption rates and/or faster diffusion of CO_2 due to their high H_2O content (Watson, 1991). Two RB samples, MGLN8-D11-8 and -D12-1, fall below the 1:1 line: they both have large vesicles with diameters between 2 and 3 mm and dissolved CO_2 contents less than 10 ppm (Table 2). It is likely that these samples experienced much slower ascent rates, allowing sufficient time for the formation of large vesicles with consequent depletion of CO_2 in

the accompanying melt. Alternatively, these samples may have been erupted at shallow water depths, degassed, and flowed down-slope to reach the depth where they were collected, or assimilated mass and/or mixed with magma characterized by a lower CO_2 content.

In the following discussion, we use $\text{CO}_2^{\text{SIMS}}$ for the comparison of CO_2 with other major volatile contents (H_2O , F, Cl, and S) because all measurements were made on the same glass chip. We use CO_2^{v} (CO_2 in vesicles as measured by the stepped heating technique) for the comparison with He isotope ratios, which were also measured by the crushing method, and thus represent volatiles captured in the vesicle phase.

4.5. H_2O

Dissolved H_2O concentrations of the Lau Basin samples vary between 0.1 and 1.9 wt% (Table 2). There are three distinctive groups in the distribution of H_2O concentrations (Fig. 8). First, most samples from the CLSC and ELSC have H_2O less than 0.5 wt%, similar to average MORB values (0.17–0.6 wt%; Jambon and Zimmermann, 1990). The exceptions are RNDB15-7-5 and RNDB15-11-8, which have extremely high H_2O contents of 0.95 and 1.15 wt%, respectively. In the case of the former sample, at least, it also has extremely high contents of Ne and Ar (Table 1) and has high Cl with respect to other ELSC samples (Table 2). Such characteristics could have been acquired through interaction with seawater. Additionally, PR and NV samples also share MORB-like water contents, with the exception of PPTU4-21-2 (PR) which has both high water and high Cl concentrations. Second, samples from MTJ have the highest H_2O contents, ranging from 0.9 to 1.9 wt%. These high water concentrations for MTJ samples are found in all lava types – basalt through andesite – so are not simply related to differentiation. Some of these samples also have high Cl concentrations. Alternatively, given the well-documented water enrichments in arc-influenced lavas compared to MORB (e.g., Wallace, 2005), there is the possibility that the water, in part, may be derived via subduction recycling: the influence of the adjacent Tonga arc on the volatile systematics of the MTJ region is discussed in Section 5.1.2. Finally, samples from the RB have intermediate water values, between 0.5 and 1.0 wt%. This range is similar to that reported for other OIB, such as Samoa (Workman et al., 2006) and Hawaii North Arch (Dixon et al., 1997). In sum, we note that the wide range in H_2O contents of the Lau Basin mirrors that reported for other back-arc basins, such as the Manus Basin (Shaw et al., 2004) and Mariana Trough (Newman et al., 2000).

4.6. Other volatiles (F, Cl, S)

Fluorine in the Lau Basin shows a wide variation – from as low as 70 ppm (CLSC) to as high as 900 ppm (MTJ). Again, there are broadly consistent patterns for different parts of the basin. The lowest concentrations (below 200 ppm) are observed in the CLSC, ELSC, PR, and NV. The two exceptions are PPTU4-21-2 (PR) and RNDB15-15-8 (CLSC) where, in both cases, high F is accompanied

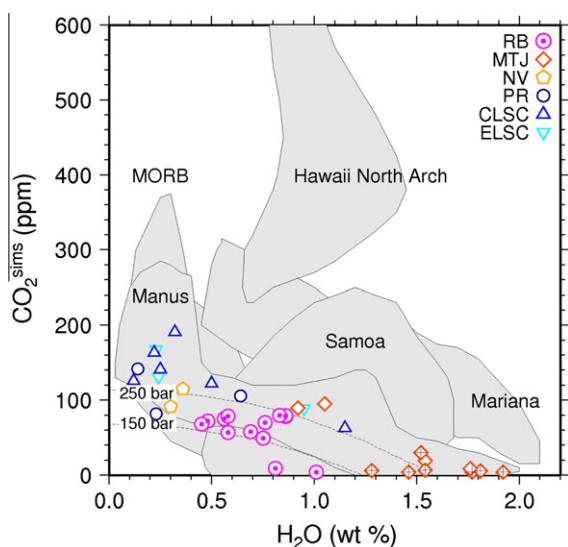


Fig. 8. Plot between $\text{CO}_2^{\text{SIMS}}$ and H_2O concentrations. Gray shades show the ranges of basaltic glasses from other studies (Dixon et al., 1997; Newman et al., 2000; Shaw et al., 2004; Workman et al., 2006). Dotted lines indicate calculated saturation concentrations at 150 and 250 bars, at which most samples were collected.

by high Cl. The MTJ has the highest F contents, with the basaltic andesites (450–770 ppm) and andesites (630–900 ppm) showing particular enrichments. The RB samples have intermediate F contents (150–480 ppm).

Fluorine is known to have a high affinity for silicate melts compared to fluid phases (Burnham, 1979; Webster, 1990). Thus, it is often found to co-vary with K_2O and/or P_2O_5 in volcanic rocks given its similar incompatibility to these species (e.g., Stecher, 1998). Such a relationship holds in the Lau Basin with F showing strong correlations with K_2O (and P_2O_5 – not shown) (Fig. 9a). The ratio of F/ K_2O is ~ 0.09 for all regions except the MTJ. This constant ratio suggests that the different regions are influenced by source magmas with more or less the same F/ K_2O ratio despite significant differences in their tectonic settings. In the case of the MTJ, however, the samples have a slightly higher F/ K_2O ratio indicating that either the F/ K_2O ratio in the source has evolved differently or is reflecting mixing with other component(s) with different F/ K_2O .

Similar patterns are seen in Cl and S contents throughout the basin. In the case of Cl, the lowest contents (<400 ppm) are characteristic of the CLSC, ELSC, PR, and NV. Only one (water-rich) sample (RNDB15-15-8) falls above this value. The MTJ has the highest Cl – again, it is the differentiated lavas which show the greatest enrichments with extreme values observed for the basalt andesites (530–1700 ppm) and andesites (2000–3800 ppm). The RB has overlapping and intermediate Cl values – from 72 to ~ 1000 ppm. As Cl and K have similar incompatibilities, the ratio Cl/ K_2O is expected to be constant during magmatic differentiation. For the most part, the Lau Basin samples display a constant ratio ~ 0.14 (Fig. 9b), consistent with fractional crystallization being the major control on the Cl contents. The principal exception to this trend is the MTJ whereby the Cl increases abruptly for a given K content (Fig. 9b). This feature is typical of shallow-level processes involving assimilation of seawater, altered oceanic crust, or brine (Kent et al., 1999). Thus, it appears that differentiated samples record the effects of extensive crustal interaction. Potential assimilants for samples with high Cl/ K_2O will be discussed in Section 5.1.

The sulfur contents in the Lau Basin samples do not vary coherently with K_2O as in the case of F and Cl. The S contents gradually increase until K_2O reaches around 0.5 wt% and then decrease with increasing K_2O contents (Fig. 9c). This trend is very similar to that of FeO^* vs. K_2O and TiO_2 vs. K_2O (not shown). Thus, the sulfur contents of Lau Basin lavas show a good correlation with FeO^* (Fig. 9d) – as do other lavas erupted at other spreading centers and seamounts (Wallace and Carmichael, 1992) – which suggests that FeO^* could be the major factor in controlling the S contents of the Lau Basin samples. Notably, non-basaltic samples from MTJ have lower S contents than other samples with the same FeO^* . This is likely due to the solubility decrease of S with diminishing Fe concentration as a result of crystallization of titanomagnetite (Moune et al., 2007). Indeed, it is known that the solubility of sulfur in magma is a complicated function of a number of parameters, such as temperature, pressure, bulk composition, fugacities of oxygen and sulfur, and the FeO content

(Wallace and Carmichael, 1992). Further consideration of the S contents is beyond the scope of this paper.

5. DISCUSSION

The isotopic composition of a particular volatile in both vesicle and glass phases, its concentration in the glass phase and its relative distribution between glass and vesicles and/or its ratio to other volatiles in both phases all offer insight into aspects of the degassing process. Relevant information to be gained includes the mode and extent of degassing, thereby allowing reconstruction of initial characteristics of the volatiles in the melt prior to gas loss. In addition, the interaction of source magmas with other volatile-carrying components such as the subducting slab (including sediment), pre-existing crust through which magmas erupt, and air/seawater may also imprint their volatile characteristics onto those of the source. In the following sections, we evaluate a number of different degassing and contamination models to assess their applicability to a greater understanding of the volatile systematics of the Lau Basin. Only following a detailed assessment of the effects of degassing and contamination, can the volatile characteristics of samples erupted in the Lau Basin be used to explore the dynamics and evolution of underlying mantle sources.

5.1. Contamination by atmosphere, crust and/or slab components

In this section, we consider contamination both from the perspective of particular volatile species and by identifying samples where there is other geochemical evidence that the samples themselves have been contaminated through various extraneous effects. In the former case, we consider the Ne and Ar systematics of the Lau samples as these two species are particularly susceptible to modification due to their typically low abundances in basaltic glasses. In the latter, our interest extends to assessing the integrity of the volatile record in spite of information from other geochemical tracers that samples may have been modified. In both cases, we are interested in identifying both individual samples and regions of the Lau Basin where contamination is particularly acute so that inferences on magma source characteristics for such samples/regions may be compromised. Conversely, those samples and regions of the Lau Basin where evidence of modification is minimal or missing may provide the best estimates of initial source characteristics of the Lau Basin mantle assuming the potentially complicating effects of degassing-induced changes can be identified and corrected.

5.1.1. Ne and Ar contamination

The effects of contamination can be acute particularly if there is a large concentration contrast between contaminant and sample. This is potentially the case for Ne and Ar due to their relatively large abundances in air and seawater vs. their low abundance in basaltic glass. We illustrate the effects of atmospheric contamination using the Ne isotope systematics of the Lau Basin samples (Fig. 10). Here, we plot the $^{20}Ne/^{22}Ne$ and $^{21}Ne/^{22}Ne$ of the samples vs. Ne concentrations. We observe that the samples with high

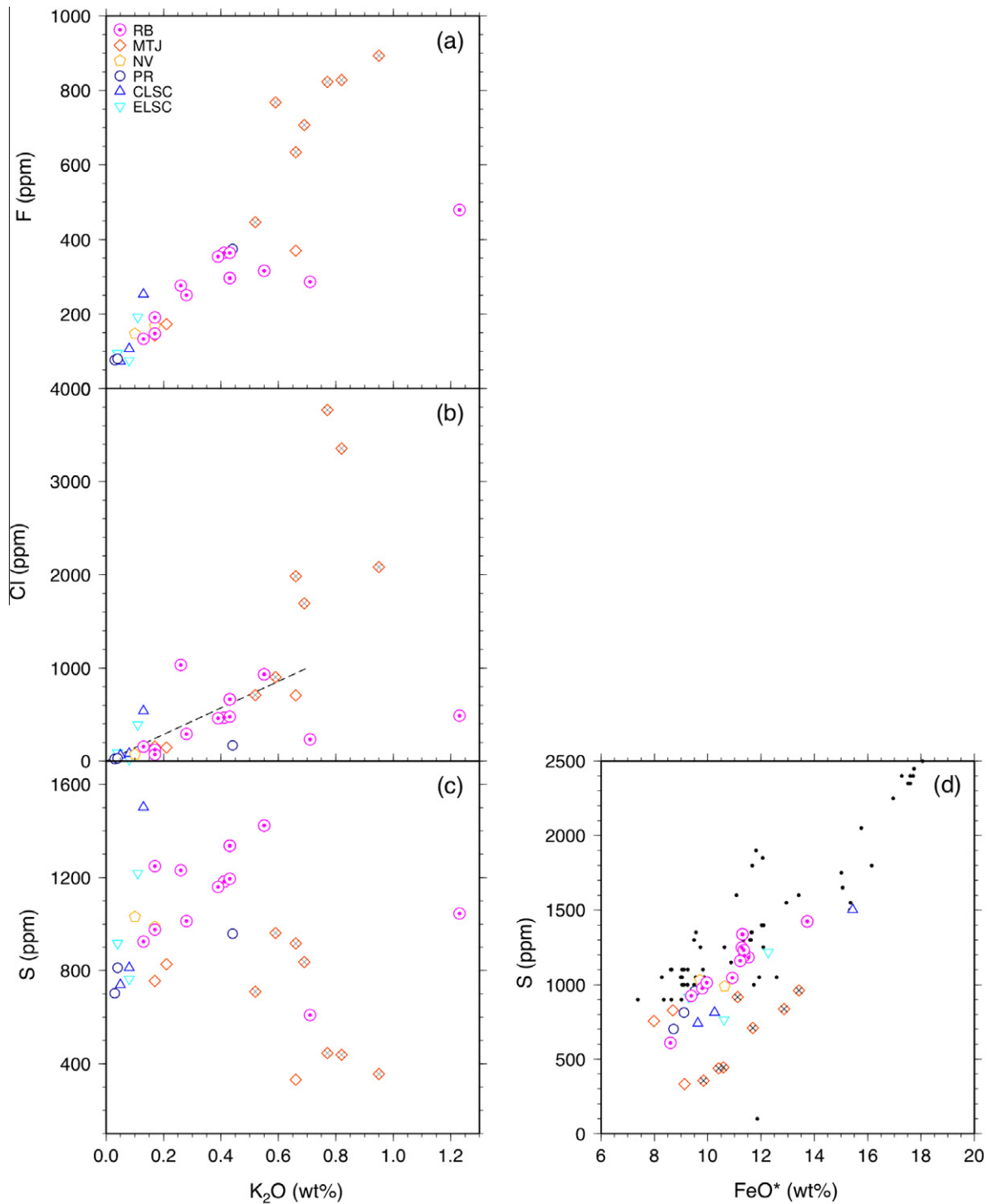


Fig. 9. Fluorine, Cl, and S vs. K_2O and S vs. FeO^* in Lau Basin samples. (a) The ratios of F/K_2O for most Lau Basin samples are fairly constant at ~ 0.09 . The ratios of MTJ samples are slightly higher. See text for discussion. (b) The ratios of Cl/K_2O for most of the samples are around 0.14 (dashed line). However, Cl of MTJ samples increases abruptly at ≥ 0.6 wt% K content. This feature is typical for shallow-level processes involving assimilation of seawater, altered oceanic crust, or brine (Kent et al., 1999). (c) The relationship between S and K_2O . The S contents gradually increase until K_2O reaches around 0.5 wt% and then decrease with increasing K_2O contents. (d) A good correlation between S and FeO^* suggests that FeO^* could be a major factor in the S contents of the Lau samples.

^{20}Ne contents (e.g., MGLN8-D11-8, -D12-1, and RNDB15-7-5 where $[Ne] > 1.7 \times 10^{-9} \text{ cm}^3 \text{ STP/g}$) have

$^{20}Ne/^{22}Ne$ and $^{21}Ne/^{22}Ne$ ratios close to atmosphere values of 9.8 and 0.029, respectively (Ozima and Podosek, 2002).

These particular samples also have high ^{40}Ar abundances and air-like $^{40}\text{Ar}/^{36}\text{Ar}$ values (Table 3). In addition, the dissolved CO_2 contents of these RB samples are very low (<10 ppm; Table 2) indicating that increased susceptibility to atmospheric/seawater contamination and extensive degassing of CO_2 (and thus noble gases) are closely linked.

Notably, however, other RB samples analyzed for Ne only possess modest shifts from atmospheric-like $^{20}\text{Ne}/^{22}\text{Ne}$ and $^{21}\text{Ne}/^{22}\text{Ne}$ values – to highs of 10.32 and 0.0314, respectively. This stands in contrast to the CLSC (this work and Honda et al., 1993b) where the majority of samples have high non-atmospheric Ne contributions ($^{20}\text{Ne}/^{22}\text{Ne}$ as high as 12.0) and low Ne concentrations (Fig. 10). Significantly, the RB samples have moderate amounts of dissolved CO_2 (50–80 ppm) – significantly higher than -D11-8, -D12-1, but not as high as CLSC and ELSC samples where the majority have dissolved $\text{CO}_2 > 100$ ppm (Table 2). Consequently, we conclude that degassed samples – resulting from shallow eruption depths, high water contents or a combination of both, possess a greater susceptibility to record the effects of air and/or seawater inputs with the caveat that the contaminating medium itself must have

significant contents of the contaminant volatile. In this respect, atmospheric and/or seawater Ne and Ar are more likely to dominate the Ne and Ar inventory of a particular sample in contrast to He and CO_2 where concentrations in the contaminant are relatively low compared to that of samples.

5.1.2. Crustal contamination: slab input vs. crustal assimilation

In addition to air/seawater contamination, it is highly likely that crustal contamination has affected at least some of the present sample suite. This could reflect addition of contaminants at the source – for example, through incorporation of a subduction component (deep contamination) – and/or assimilation by components within the over-riding crust through which magmas are erupted (shallow contamination). Tian (2011) argues for variable subduction contamination throughout the Lau Basin. However, Kent et al. (2002) noted that Cl enrichment in MTJ and VFR lavas was well correlated with high Ba/Nb and U/Th ratios whereas this was not the case for the CLSC and ELSC. Hence, they argued that slab-derived fluids from the proximal Tonga subduction zone were responsible for the Cl enrichment in the former locations whereas assimilation of altered (chlorine-rich) ocean crust occurred at the latter sites.

In Fig. 11a, we plot K_2O -normalized Cl contents vs. Ba/Nb for all Lau Basin samples. Because Ba is more mobile than Nb in slab-derived fluids (Brenan et al., 1995), an increase in Ba/Nb is a sensitive indicator of subduction-related (deep) components (Kent et al., 2002). We find substantial differences in Ba/Nb ratios among the Lau Basin sample suite: PR and NV samples have the lowest range (0–4), CLSC has values from 5 to 7 and ELSC falls between 8 and 11. The higher Ba/Nb of ELSC relative to CLSC is consistent with the influence of a modest subduction component in the ELSC mantle source presumably because it is closer to the Tonga Arc than the CLSC (cf., Tian et al., 2008; Escrig et al., 2009). RB samples roughly overlap with CLSC/ELSC samples (excluding anomalous PPTU4-23-2, MGLN8-D12-1, and -D9-9) whereas MTJ samples have the highest range of values (13–19). In this respect, the MTJ samples present the most compelling evidence for the presence of a subduction component in the region. However, the differentiated samples of the MTJ show a large enrichment of Cl ($\text{Cl}/\text{K}_2\text{O} > 0.2$) which is not accompanied by an increase in Ba/Nb (Fig. 11a). Thus, we concur with Kent et al. (2002) that MTJ lavas possess a strong subduction influence but it is unlikely that the Cl enrichment is also due to the influence of the subducting slab since there is no obvious correlation between $\text{Cl}/\text{K}_2\text{O}$ and Ba/Nb. Indeed, it is more likely that other assimilation processes are responsible for the Cl enrichment.

This conclusion is reinforced by plotting Cl/Nb vs. Ba/Nb (Fig. 11b) which has the advantage of using the same denominator on both axes so that additions of Cl (relative to Ba) can be observed directly. For the most part, there is a good positive correlation between these two parameters for Cl/Nb ratios $< \sim 120$. This includes samples from the PR, NV, RB, CLSC and undifferentiated samples from the

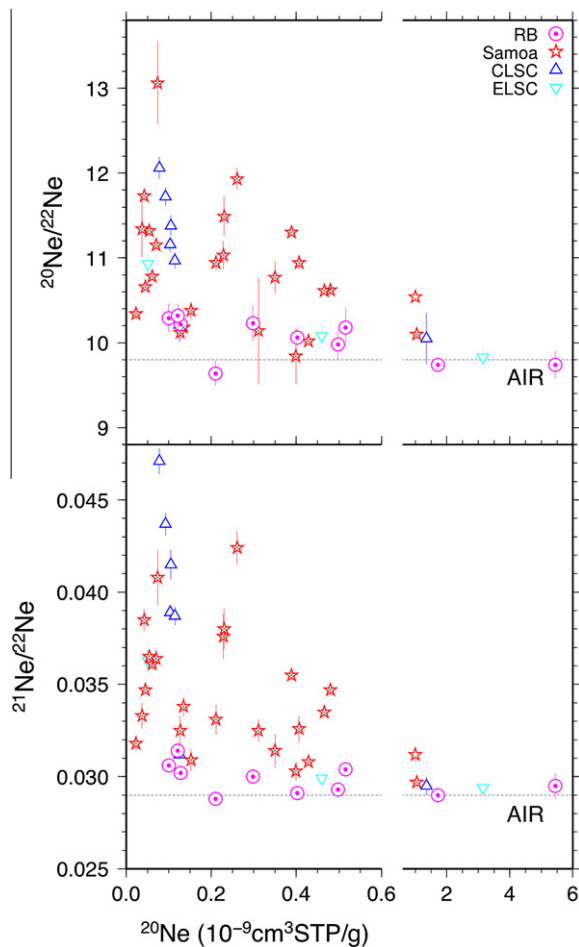


Fig. 10. The relationships between Ne isotope ratios and ^{20}Ne abundance. The dashed lines represent the atmospheric ratios of $^{20}\text{Ne}/^{22}\text{Ne}$ and $^{21}\text{Ne}/^{22}\text{Ne}$ of 9.8 and 0.029, respectively (Ozima and Podosek, 2002). The Samoa and some of the CLSC results are from Poreda and Farley (1992) and Honda et al. (1993b), respectively.

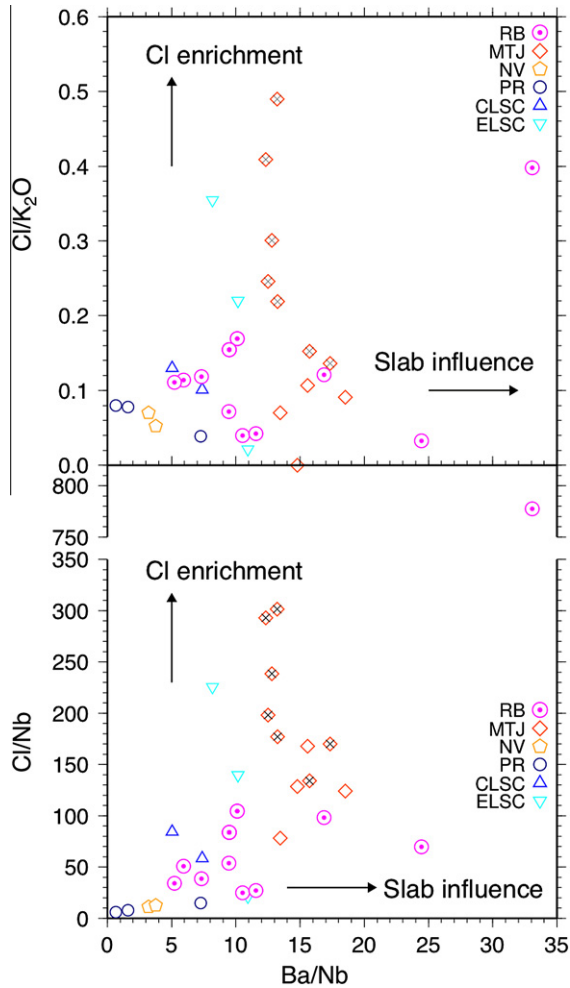


Fig. 11. Chlorine/potassium (upper) and chlorine/niobium (lower) vs. barium/niobium ratios for Lau Basin samples. Note that the MTJ samples (diamonds) have high Ba/Nb than samples from other regions, suggesting a significant slab-influence. They also have high Cl/K₂O (>0.2). Given no correlation between Cl/K₂O and Ba/Nb, the Cl enrichment is likely due to assimilation of Cl-rich material rather than slab-influence.

MTJ. In contrast, differentiated MTJ samples plus two ELSC (RNDB15-5-8; -7-5) and one RB sample (PPTU4-23-2) have significantly higher Cl/Nb for a given Ba/Nb ratio consistent with addition of extraneous (shallow) Cl from either seawater, altered crust or associated brines (e.g., Kent et al., 1999). In summary, a few samples with high Ne abundances (for example, MGLN8-D11-8, -D12-1, and RNDB15-7-5) show atmospheric Ne and Ar isotopic ratios, which can be attributed to the contamination with seawater and/or an atmospheric component. On the other hand, many samples, particularly from the MTJ, are likely to be contaminated by a subduction component and/or Cl enriched materials such as seawater, altered crust or brines. Specifically, we regard the following samples as contaminated: all five MTJ andesites and basaltic andesites samples (see the footnote of Table 1) and two basalts from the ELSC, based on their high Cl/K₂O. Thus, in the following discussion, we pay particular attention to samples and loca-

tions (MTJ and ELSC) where there is evidence for contamination and contrast them with other samples where indications of modification are minor or equivocal at best.

5.2. Constraints on CO₂ degassing: glass phase data

In this section, we consider the volatile systematics of the dissolved, i.e., glass, component to ascertain its applicability to deciphering the degassing history of the Lau Basin samples reported here. Volatiles dissolved in the glass phase can be considered as being residual following gas loss via vesiculation. In this case, we can use the concentration of CO₂ and its δ¹³C to model the initial CO₂ content of the melt phase and its degassing history (e.g., Macpherson and Matthey, 1994). However, as noted in Section 4.4, δ¹³C^d > δ¹³C^v, i.e., Δ-values are negative for most of the present sample suite, indicating that pure equilibrium degassing conditions assuming either batch equilibrium degassing (BED) or fractional equilibrium degassing (FED) modes alone do not provide an adequate description of gas loss from the samples (see also Shaw et al., 2004; Macpherson et al., 2005). This can be seen in Fig. 12a where many samples lie in the region in-between the two end-member degassing trajectories. In this case, we can assume that samples have undergone a two-stage gas loss, first involving BED followed by FED. This approach has proven successful for describing the degassing process at Kilauea and other localities (e.g., Pineau and Javoy, 1983; Gerlach and Graeber, 1985) as well as for the Lau Basin (Macpherson and Matthey, 1994).

In the following, we adopt the methodology of Macpherson and Matthey (1994) who assumed that any given measured CO₂ concentration and isotopic composition could result from either BED and/or FED. Since FED generally produces larger fractionations, and thus lower δ¹³C values, it is assumed that glasses with the lowest δ¹³C values resulted from FED and that glasses with the highest δ¹³C values have experienced BED. In detail, the following equations apply:

$$d_{rBED} = d_p - \Delta(1 - (C_{rBED}/C_p)) \quad (1)$$

$$d_{rFED} = d_p + \Delta \ln(C_{rFED}/C_p), \quad (2)$$

where d_{rBED} and d_{rFED} represent the isotopic composition of CO₂ remaining dissolved in the melt for BED and FED, respectively, C_{rBED} and C_{rFED} are the concentrations of residual CO₂ for BED and FED, C_p and d_p are the concentration and isotopic composition of dissolved CO₂ of the pre-eruptive melt, and Δ is isotopic fractionation between gas and melt ($\Delta = \delta^{13}C_g - \delta^{13}C_m$). Assuming that all the samples have been degassed from a common pre-eruptive melt with the same C_p and d_p , any particular d_r occurs at two residual concentrations (C_{rBED} or C_{rFED}) depending on the degassing style. At this particular d_r (i.e., $d_{rBED} = d_{rFED}$), Eqs. (1) and (2) can be combined as $\ln C_p + (C_{rBED}/C_p) = 1 + \ln C_{rFED}$. By combining two residual melts which have different residual isotopic compositions and concentrations – ($d_r^1, C_{rBED}^1, C_{rFED}^1$) and ($d_r^2, C_{rBED}^2, C_{rFED}^2$), C_p can be estimated using:

$$C_p = (C_{rBED}^1 - C_{rBED}^2) / \ln(C_{rFED}^1/C_{rFED}^2) \quad (3)$$

The principal question that we attempt to address with this approach is whether there is any evidence of CO₂ heteroge-

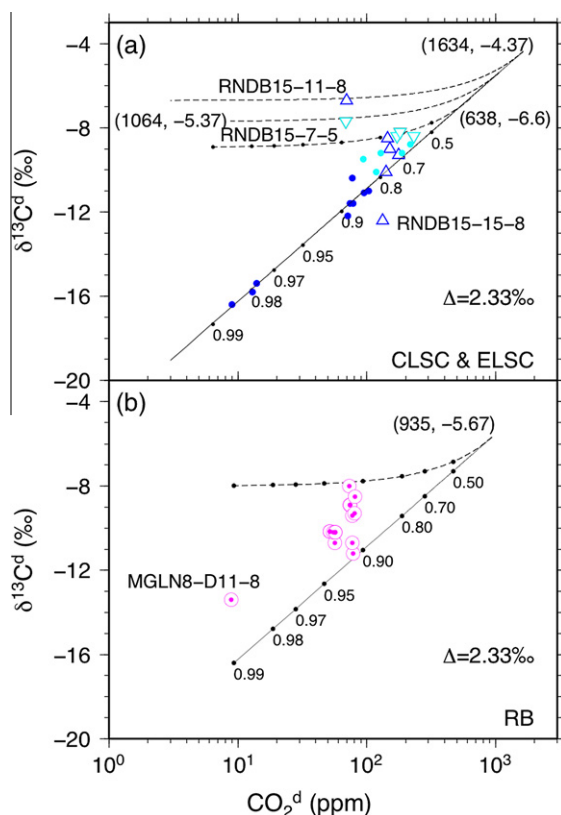


Fig. 12. Dissolved CO₂ content and C isotopic ratios in (a) CLSC/ELSC and (b) RB, superimposed on BED (dashed lines) and FED (solid lines) trajectories from source melts. The small black dots on the trajectories show the degree of degassing from the source (638 ppm, -6.6‰) and (935 ppm, -5.67‰) in (a) and (b), respectively. The cyan and blue dots in plot (a) are from Macpherson and Matthey (1994). (For interpretation of the references to color in this figure legend, the reader is referred to the web version of this article.)

neity in primary melts (prior to degassing) for the various parts of the Lau Basin where we have obtained CO₂ data.

We begin with samples from the CLSC where there are numerous samples which have a wide range of carbon isotope and CO₂ concentrations (Table 2 and Macpherson and Matthey, 1994). Additionally, we use the regression plot of Macpherson and Matthey (1994) which, with the exception of one sample (see below), provides a robust limit to FED of all samples including those analyzed as part of this study (Fig. 12a). However, as is clear from Eq. (3), two different sets of carbon concentration and isotopic data that fall on a BED trajectory are required to estimate C_p , and there is no clear choice in the entire CLSC database. Therefore, we choose to combine the ELSC and the CLSC database and select RNDB15-5-8 ($C_{rBED}^1 = 171.9$ ppm, $d_r^1 = -8.4\text{‰}$) and RNDB15-35-1 ($C_{rBED}^2 = 144.5$ ppm, $d_r^2 = -8.5\text{‰}$) as two samples which follow a BED trajectory. In this way, C_{rFED}^1 and C_{rFED}^2 can be calculated using the FED regression line ($d_r = 2.33 \ln(C_{rFED}) - 21.6$) derived from Macpherson and Matthey (1994). We use $\Delta = 2.33\text{‰}$ for the calculation, which is also the same as the slope of FED regression line above. This gives us C_{rBED}^1 and C_{rFED}^1 as well as C_{rBED}^2 and C_{rFED}^2 , thus en-

abling us to estimate C_p and then d_{rBED}^1 , d_{rBED}^2 , d_{rFED}^1 , and d_{rFED}^2 using Eqs. (1) and (2) – see Appendix B. The estimated CO₂ composition of pre-eruptive melt is 640 ppm, with a $\delta^{13}C$ value of -6.6‰ . In comparison, the database of Macpherson and Matthey (1994) alone produced an estimate of 410–440 ppm and -7.7‰ , for CO₂ and $\delta^{13}C$, respectively, in the central Lau Basin. We note that the above approach assumes that parental melt in the CLSC and ELSC have similar CO₂ characteristics: if there is no recycling of subduction-related CO₂ to the back-arc, as recently concluded by Macpherson et al. (2010), then this strengthens the case for treating CLSC/ELSC together.

An estimate of the degree of uncertainty associated with this estimate of C_p can be gained by noting that the anticipated precision on the isotopic composition of any given sample is likely to be of the order of $\pm 0.4\text{‰}$, based upon repeat analyses of our internal (house) standard glass ALV981-R23 (Macpherson et al., 1999). Thus, a highly degassed sample by BED would be expected to have a d_r value of $-8.93 \pm 0.4 \text{‰}$ (i.e., $-6.6\text{‰} - \Delta$) which, by forward modeling, would lead to the same uncertainty on the estimate of d_p (i.e., $-6.6 \pm 0.4\text{‰}$). If the empirical FED relationship of $d_r = 2.33 \ln(C_{rFED}) - 21$ holds true (see above) then the lower extreme of d_p (-7.0‰) produces a C_p value of 530 ppm whereas the higher estimate (-6.2‰) gives 750 ppm. In other words, we estimate the uncertainty on C_p at ± 120 ppm ($\sim 17\%$). Our estimates of both concentration and isotope values of predegassed melt carbon of the ELSC/CLSC, taking into account the degrees of uncertainty, fall close to those of MORB. For example, Sano and Marty (1995) adopt a value of -6.5‰ for the carbon isotope composition of MORB, and Saal et al. (2002) estimate a primary MORB magma CO₂ content of 720 ppm.

Although most of the ELSC/CLSC CO₂ data can be described by the above two-stage degassing model, there are three obvious outliers that plot outside the bounding BED and FED trajectories in Fig. 12a. Sample RNDB15-15-8 (ELSC) falls below the well-defined FED trajectory, and is possibly contaminated by interaction with crust. This sample has the highest F, S, and Cl among all the CLSC samples (Table 2). Two samples with high $\delta^{13}C$, (RNDB15-11-8 and -7-5), fall above the BED line and stand alone, i.e., are not accompanied by other samples that could possibly follow a BED trajectory. For both these samples, therefore, C_p cannot be determined analytically but can be approximated using a graphical approach. If we assume that degassing is sufficiently advanced ($>90\%$) so that the change in $\delta^{13}C$ from the initial value is approximately equal to Δ (2.33‰) then we can project back to the FED trajectory and estimate C_p . For samples RNDB15-11-8 and RNDB15-7-5, we obtain values of 1600 and 1100 ppm, respectively. However, we caution that these two estimates are predicated on single samples only with no other data points to confirm degassing trajectories: therefore, these estimates must be viewed with skepticism. In this respect, we have much greater confidence in the previous estimate of C_p (640 ppm and -6.6‰) given the greater number of samples that define the empirical FED trajectory.

Using the same methodology as above, we plot the RB samples in Fig. 12b. However, in this case, there is no obvi-

ous trend in $\delta^{13}\text{C}$ vs. $\log \text{CO}_2$ that can help us define the FED trajectory. Therefore, as a first approximation, we adopt the same FED trajectory as defined for the CLSC (Fig. 12a) and note that it provides a reasonable bounding limit to the RB dataset (Fig. 12b). By again assuming that the sample with the highest $\delta^{13}\text{C}$ value (MGLN8-D9-9; -8.0‰) has undergone pure BED, we can plot the intersection of the BED trajectory with the FED curve at a value equal to C_p . For the case of the RB, the estimate of pre-degassed melt composition is 940 ppm CO_2 and $\delta^{13}\text{C} = -5.7\text{‰}$. By treating the degree of uncertainty in the same manner as for the ELSC/CLSC (i.e., $\sim 17\%$ on C_p and $\pm 0.4\text{‰}$ on d_p) then, the C content of RB at 940 ± 170 ppm is still higher than that of the combined CLSC/ELSC estimate (lower limit of RB = 770 ppm vs. an upper limit of 750 ppm). We note, however, the RB estimate is much lower than that of Kilauea source melt (3200–6500 ppm; Gerlach and Graeber, 1985; Greenland et al., 1985). Additionally, the RB $\delta^{13}\text{C}$ melt estimate is higher than that of the CLSC/ELSC, but is in agreement with tholeiites from Loihi Seamount ($\sim -5.0\text{‰}$; Exley et al., 1986) – which also erupts high ${}^3\text{He}/{}^4\text{He}$ lavas. However, we again caution that these perceived differences in CO_2 and $\delta^{13}\text{C}$ values between the CLSC/ELSC and RB are highly model dependent and should be viewed as illustrative and not necessarily definitive.

5.3. Vesicle-sited gas: evidence of assimilation

Gases stored in vesicles of oceanic glasses are produced through oversaturation of particular volatile species in the melt phase leading to formation of a separate vapor phase co-existing along with the melt. The cause of the oversaturation is primarily reduction in confining pressure as magma moves towards the surface which leads to lowering of the solubility of a volatile species. However, magma crystallization (i.e., volume reduction) and changes in magma composition can also exert a control on vapor generation within a melt. Given differences in the solubility of various volatile species in the melt phase, formation of a vapor phase invariability leads to elemental fractionation between volatile species. In the case of CO_2 , an accompanying isotopic fractionation can be produced due to the formation of molecular CO_2 in the vapor phase from carbonate ion complexes dissolved in the melt (Harris, 1981; Fine and Stolper, 1986; Javoy and Pineau, 1991). An added complication in understanding the origin(s) of vesicle-sited volatiles is that open system conditions may prevail, e.g., by differential movement of vesicles and melt, so that different populations of vesicles representing different stages of degassing may merge and/or become trapped within a given aliquot of glass. In spite of these caveats, considerable information is available from the vesicle-sited volatile component of the Lau Basin database. To this end, we plot combinations of the following elemental ratios found in the vesicle phase – ${}^4\text{He}/{}^{40}\text{Ar}^*$, $\text{CO}_2/{}^{40}\text{Ar}^*$ and $\text{CO}_2/{}^3\text{He}$ (Fig. 13). Furthermore, we make the assumption that the sample with the lowest ${}^4\text{He}/{}^{40}\text{Ar}^*$ ratio (MGLN8-D9-9 where ${}^4\text{He}/{}^{40}\text{Ar}^* = 4.9$) is the least degassed sample, and thus provides a useful starting point to consider (further) degassing

associated with eruption of the Lau samples onto the seafloor. As the (mantle) production ratio of ${}^4\text{He}/{}^{40}\text{Ar}^* \sim 2$ (Marty and Zimmermann, 1999), MGLN8-D9-9 must have experienced some prior volatile degassing, most likely associated with the transfer process from the mantle source to shallower reservoirs in the crust. We note that this assumption is consistent with the isotope and abundance systematics of carbon in the dissolved phase of this sample (Section 5.2) which also indicates gas loss.

In Fig. 13, elemental ratios of vesicle-sited volatiles (${}^4\text{He}$, ${}^{40}\text{Ar}^*$ and CO_2) are plotted taking advantage of the fact that differences in the solubility of the three species in basaltic melt lead to elemental fractionation during vesicle formation. Consequently, we can plot equilibrium degassing trajectories for both BED and FED from a presumed starting composition (given by sample MGLN8-D9-9). Relative solubilities in basaltic melt of 2.4 ($S_{\text{He}}/S_{\text{CO}_2}$; Hilton et al., 1998) and 4 ($S_{\text{CO}_2}/S_{\text{Ar}}$; Cartigny et al., 2001) produce increases in ${}^4\text{He}/{}^{40}\text{Ar}^*$ and $\text{CO}_2/{}^{40}\text{Ar}^*$ and a decrease in $\text{CO}_2/{}^3\text{He}$ in the residual phase as degassing progresses. For BED trajectories (lines labeled 0), we use the equation for the residual volatiles as this is appropriate for multi-stage vesiculation and vesicle loss. As demonstrated previously (e.g., Jambon et al., 1986), the residual volatiles are transferred to subsequent generations of vesicles, and thus vesicle data display elemental fractionation trends that can be fitted by equations that hold for the residual volatile phase. As seen in all three sub-plots of Fig. 13, BED and FED degassing trajectories (or a combination thereof) starting from sample MGLN8-D9-9 (lines labeled 0 and 1, respectively) provide a reasonable fit to the majority of the RB samples. However, this is not the case for two low $\text{CO}_2/{}^3\text{He}$ (MGLN8-D10-2 from RB and RNDB-15-26-1 from CLSC) and two high $\text{CO}_2/{}^3\text{He}$ samples (MGLN8-D7-25 and MGLN8-D7-25b, both from the RB). Thus, we can conclude that the majority of Lau Basin samples studied here has experienced degassing, likely at a relatively late stage prior to eruption, with the vesicles capturing volatiles exsolved from previously degassed magma. In most cases, they share a common starting composition provided by sample MGLN8-D9-9. However, the four outlier samples require a different explanation.

There are two samples with distinctly high $\text{CO}_2/{}^3\text{He}$ values ($> 3 \times 10^{10}$): such high values cannot be induced by degassing alone as resultant $\text{CO}_2/{}^3\text{He}$ ratios would be lower than plausible starting values (Fig. 13). Addition of extraneous CO_2 is the likeliest explanation with a plausible mechanism being assimilation of wall rock CO_2 by melts en route to the surface. Notably, because the glass phase $\delta^{13}\text{C}$ – CO_2 systematics of samples MGLN8-D7-25 and MGLN8-D7-25b conform to equilibrium degassing (Fig. 12), we can deduce that the extraneous CO_2 must be isotopically similar to that of the magma (see further discussion in Macpherson et al., 2010). Furthermore, if previously-degassed sample MGLN8-D9-9 can still provide a plausible starting composition for these two samples then it points to a relatively shallow location (crustal magma chamber?) where the CO_2 assimilation occurred. We can test this possibility by using the coupled assimilation-fractionation degassing model of Macpherson et al. (2010).

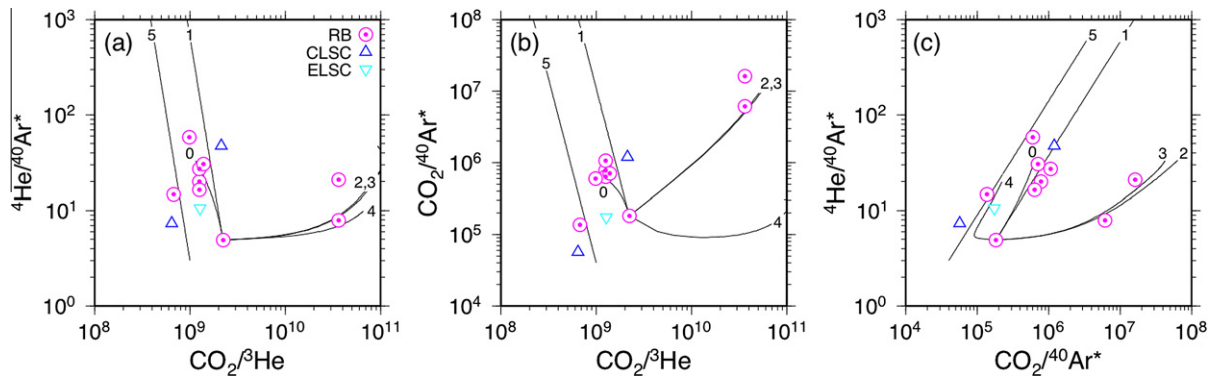


Fig. 13. The relationships among elemental ratios in the vesicle phase of RB samples (circles with dot). Lines 0 and 1 show batch and fractional equilibrium degassing from elemental ratios of MGLN8-D9-9. Lines 2, 3 and 4 show fractional degassing with assimilation of pure CO_2 and CO_2 with $^3\text{He}/^4\text{He}$ of 8 and 0.05 R_A , respectively. For coupled degassing/assimilation from D9-9, we assume the assimilant is characterized by $\text{CO}_2/{}^3\text{He}$ of 2.2×10^{11} (100 times enriched compared to D9-9), ${}^4\text{He}/{}^{40}\text{Ar}^*$ of 4.9 (equal to D9-9) and assimilated CO_2 :degassed CO_2 ratio equal to the enrichment factor (i.e., 100). Line 5 shows fractional degassing from an alternative source melt with $\text{CO}_2/{}^3\text{He}$, ${}^4\text{He}/{}^{40}\text{Ar}^*$, and $\text{CO}_2/{}^{40}\text{Ar}^*$ of 1.0×10^9 , 3.0, 4.0×10^4 , respectively.

The coupled assimilation–fractionation degassing model assumes loss of CO_2 in 1% increments by FED from a given starting composition (in this case provided by MGLN8-D9-9). This step is followed by addition of assimilant CO_2 , enriched by a factor of 100 over the initial $\text{CO}_2/{}^3\text{He}$ ratio. The ratio of assimilated CO_2 to degassed CO_2 is assumed to be the same as the enrichment factor. The degassing step is then repeated from the new starting composition. The results of this model are plotted in Fig. 13a–c as lines labeled ‘2’. Modifications of the assimilant characteristics to include isotopic variability in ${}^3\text{He}/{}^4\text{He}$ ratios (at 8 R_A and 0.05 R_A) are plotted as lines 3 and 4, respectively. As can be seen in the various plots, both lines 2 and 3 provide reasonable approximations for the two high $\text{CO}_2/{}^3\text{He}$ samples – for all three elemental ratios: however, this is not the case for trajectory 4 due to its inability to replicate measured $\text{CO}_2/{}^{40}\text{Ar}^*$ ratios (plots 13b and c). Thus, we can recognize extensive wall rock interaction as an important control on the volatile systematics in some parts of the RB. Moreover, the characteristics of the wall rock do not include an aged component, as there is no evidence that radiogenic He ($\sim 0.05 R_A$) is added to the melt.

This leaves two other samples (MGLN8-D10-2 from RB and RNDB-15-26-1 from CLSC) that cannot be explained by degassing alone (from MGLN8-D9-9) or through coupled assimilation-fractional degassing: both samples possess low (vesicle) $\text{CO}_2/{}^3\text{He}$ ratios. Heterogeneity in elemental source characteristics is one possible explanation, particularly for the RB where extensive variations in ${}^3\text{He}/{}^4\text{He}$ are observed (Fig. 2). For example, if the source melt had ${}^4\text{He}/{}^{40}\text{Ar}^*$, $\text{CO}_2/{}^{40}\text{Ar}^*$ and $\text{CO}_2/{}^3\text{He}$ characteristics of 3.0, 4.0×10^4 and 1.0×10^9 , respectively, then both samples could be explained by FED alone (line 5 in Fig. 13a–c). However, recent studies have suggested that $\text{CO}_2/{}^3\text{He}$ ratios of high ${}^3\text{He}/{}^4\text{He}$ mantle (i.e., ${}^3\text{He}/{}^4\text{He} >$ MORB) are equal to or greater than MORB-like values of $\sim 2 \times 10^9$ (see discussion in Shaw et al., 2004) so this effectively rules out this possibility, at least for the RB sample. An added complication in the case of the RB sample is

that it may have come from a mixed source consisting of material from the Samoan plume and pre-existing, subduction component-metasomatized back-arc basin mantle (Tian, 2011). Alternatively, a mechanism is required to produce lower $\text{CO}_2/{}^3\text{He}$ (and $\text{CO}_2/{}^{40}\text{Ar}^*$) values with minimal effect on ${}^4\text{He}/{}^{40}\text{Ar}^*$ ratios – thus shifting these two samples from their location close to the majority of the RB samples (in Fig. 13a–c). Such a mechanism is not obvious but we can speculate that sample preparation could have a role. For example, this would require both a wide variation in vesicle size distribution in these two samples and loss of large vesicles through selection of small pieces of glass. The large vesicles would then have to contain relatively high CO_2 contents (with respect to ${}^3\text{He}$ and ${}^{40}\text{Ar}^*$): a condition met by selective assimilation of pure CO_2 by the largest vesicles in the magma.

In summary, the elemental characteristics of vesicle-sited volatiles are compatible with degassing of a parental magma which itself is partially degassed relative to that postulated for the mantle source. The parental magma is likely stored in crustal magma chambers where addition of CO_2 can occur in some instances. The mechanism of CO_2 addition is probably wall rock interaction, which can act to supersaturate melts and thus promote vesiculation.

5.4. CO_2/Nb ratios and inferences on the Lau Basin mantle

Considerable attention has been focused on CO_2/Nb ratios in oceanic basalts due to the similar incompatibilities of these two elements upon melting and hence preservation of their relationship in the mantle source. Saal et al. (2002) found that olivine-hosted melt inclusions in MORB from the Siqueiros transform fault (EPR) had quasi-constant CO_2/Nb ratios of 239 ± 46 and this could be combined with estimates of the MORB source Nb content (0.3 ± 0.05 ppm; Hofmann, 1988) to yield a value of 72 ± 19 ppm for the source CO_2 content. At 10% partial melting, the anticipated concentration of CO_2 in the primary melt is 720 ppm. In this section, we consider the

CO₂/Nb systematics of various regions of the Lau Basin to assess its variability throughout the Lau Basin for comparison with other ridge (e.g., mid-Atlantic Ridge – Cartigny et al., 2008; Gakkel Ridge – Shaw et al., 2010) and hotspot settings (e.g., Galapagos Islands – Koleszar et al., 2009).

There is a wide range in measured CO₂/Nb ratios for samples from the Lau Basin (Table 2). The range of values is 0.45–56.4 (RB), 0.35–76 (MTJ), 9.2–35.4 (PR), 13.0–18.4 (NV), 102–164 (CLSC) and 51–210 (ELSC); the highest value is 210 (RNDB15-31-1; ELSC) and the lowest is 0.35 (RNDB15-20-7; MTJ). Estimated uncertainties on these ratios are <6% assuming reproducibility of $\sim\pm 2\%$ (Macpherson et al., 1999) and $\sim 5\%$ (Table 2) on CO₂ and Nb, respectively. Therefore, all values are below the Siqueiros benchmark value of 239 for depleted MORB mantle (Saal et al., 2002). Observations of low CO₂/Nb ratios in quenched glasses have been reported previously (e.g., Saal et al., 2002; Koleszar et al., 2009; Shaw et al., 2010), and are not unexpected given arguments presented previously (Section 5.2) that CO₂ is extensively degassed from Lau Basin samples in this study. The pertinent question is whether it is possible to estimate unmodified CO₂/Nb values for the present sample suite, also taking into account the wide variations in Nb contents (Table 2).

In Fig. 14a–c we plot diagnostic element concentrations and ratios (MgO, Cl/K₂O and Ba/Nb indicating differentiation, crustal contamination and slab involvement, respectively) vs. Nb to assess how these processes can affect Nb contents. Additionally, Fig. 14d–f shows three key volatile concentration plots (H₂O, CO₂ and F, respectively) against Nb to further consider controlling factors on Nb contents. The general incompatibility of Nb can be seen by the inverse correlation with MgO content (Fig. 14a) and generally positive correlations with incompatible volatiles H₂O and F (Fig. 14d and f, respectively): however, there are other factors affecting Nb content. As discussed in Section 5.1.2, a number of samples have experienced crustal contamination and/or have evidence for slab involvement in the source: such indices, Cl/K₂O (Fig. 14b) and Ba/Nb (Fig. 14c), respectively, appear to correlate either positively or very little with Nb content, respectively, suggesting the crustal contamination is a predominant influencing factor. It is therefore possible to identify a number of samples from the RB with relatively unmodified Nb contents (i.e., those with low H₂O, F and Cl/K₂O and high MgO, such as MGLN8-D9-9, -D10-2 and PPTU4-23-2) and those with higher, modified values (e.g., MGLN8-D11-8, PPTU4-24-1). Likewise, the CLSC and ELSC samples have Nb contents which can be considered relatively unmodified with the possible exception of RNDB15-7-5 (ELSC) which has high H₂O and F and low MgO. The other samples suites in the basin either display evidence of little (PR and NV) or significant modification (MTJ) of Nb but, unfortunately, there are too few samples within each of these suites to reconstruct primary melt CO₂ contents (Section 5.2).

Identification of a number of Lau Basin samples with Nb contents relatively unmodified by extraneous effects allows assessment of the primary melt CO₂/Nb ratios – assuming degassing loss of CO₂ is the sole factor contributing to variations in measured CO₂/Nb values. For this reconstruction, we use the average value derived for undegassed melt CO₂

content (Section 5.2) as opposed to correcting individual samples as carried out by Cartigny et al. (2008) given that most samples of this study have $\delta^{13}\text{C}^{\text{d}} > \delta^{13}\text{C}^{\text{v}}$, i.e., Δ -values ($=\delta^{13}\text{C}^{\text{v}} - \delta^{13}\text{C}^{\text{d}}$) are negative (Section 4.4), and not +3.5% as assumed by Cartigny et al. (2008).

Thus, we adopt a value of 940 ± 170 ppm for the RB (i.e., $\sim 18\%$ uncertainty reflecting uncertainties on both inferred parental magma CO₂ (Section 5.2) and Nb (Table 2)), giving primary melt CO₂/Nb values of 580 ± 110 , 410 ± 70 and 700 ± 130 for samples MGLN8-D9-9, -D10-2 and PPTU4-23-2, respectively. All three samples have ³He/⁴He values >MORB, up to 14.1 R_A for PPTU4-23-2 (Table 1). Thus, all three samples have estimated CO₂/Nb ratios significantly higher than depleted MORB (239 ± 46 ; Saal et al., 2002). A similar approach for samples with MORB-like ³He/⁴He ratios (8 ± 1 R_A) from the CLSC and ELSC – assuming undegassed melt CO₂ contents of 640 ± 120 ppm (Section 5.2) produces even higher estimates of CO₂/Nb ratios for select samples. For example, RNDB15-26-2 and -27-1 (CLSC) yield CO₂/Nb values of 830 ± 150 and 460 ± 80 , respectively, whereas ELSC samples RNDB15-31-1 and -15-5-8 give ratios of 800 ± 140 and 1010 ± 180 , respectively. Based on low to moderate Ba/Nb ratios of these CLSC and ELSC samples, it seems unlikely that slab involvement is a major control on these high CO₂/Nb values.

We conclude, therefore, that the different regions of the Lau Basin appear to be characterized by a range of primary CO₂/Nb in the mantle source – assuming the ratios remain unfractionated during melt production. This may not be surprising given the notion that the mantle beneath the Lau Basin is heterogeneous as it may have experienced complex geochemical depletion processes associated with back-arc magmatism and incursion of Indian mantle from the north (e.g., Pearce et al., 2007). An important finding of this study is that CO₂/Nb values are generally higher than initial estimates of depleted MORB-source (Saal et al., 2002), in agreement with conclusions of Cartigny et al. (2008) who suggested CO₂/Nb values could be as high as 730 at 34°N on the mid-Atlantic Ridge. More significantly, there is no evidence for a systematic difference in CO₂/Nb ratios between mantle sources characterized by high and lower (MORB-like) ³He/⁴He ratios, i.e., between RB and ELSC/CLSC sample suites.

5.5. He–Ne systematics of the Lau Basin mantle

Although mantle sources supplying melts to the RB and ELSC/CLSC regions of the Lau Basin have overlapping values of CO₂/Nb, this is clearly not the case for He isotopes (Section 4.1) or Ne isotopes (Section 4.2). Indeed, the presence of ³He/⁴He ratios in the RB > MORB-like values provides powerful arguments in favor of the flow of plume-type mantle into the northern Lau Basin mantle through a tear in the Pacific Plate (Turner and Hawkesworth, 1998). However, there is a wide range of ³He/⁴He values in the northwestern Lau, from 28 R_A in the RR to ~ 9 R_A along the PR (Section 4.1). In this section, we address the likely cause of this wide variation by coupling He isotope measurements with our new Ne isotope data obtained on the same samples (Section 4.2). This approach

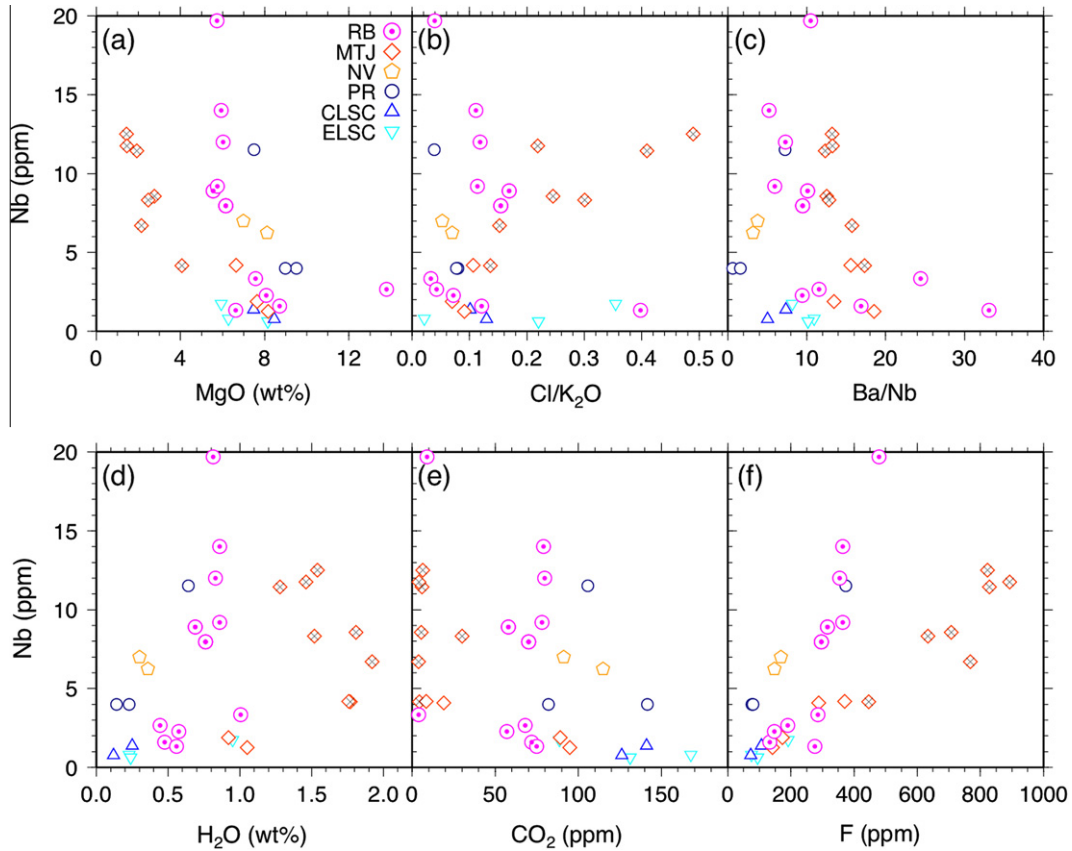


Fig. 14. Niobium vs. MgO, selected elemental ratios, and volatile contents of the Lau Basin samples.

allows us to test whether binary mixing between plume-type and MORB-like mantle can explain the He–Ne variations seen in the RB and other regions of the Lau Basin and, if so, to assess the He/Ne characteristics of the end-members involved.

An essential prerequisite of testing the binary mixing model is correcting for air-contamination, which is omnipresent to neon isotope measurements. We use measured $^{21}\text{Ne}/^{22}\text{Ne}$ values extrapolated to ‘solar’ neon isotope ratios (hereafter $^{21}\text{Ne}/^{22}\text{Ne}_{\text{EX}}$) to derive air-corrected values using the following equation (Graham, 2002):

$$^{21}\text{Ne}/^{22}\text{Ne}_{\text{EX}} = (^{21}\text{Ne}/^{22}\text{Ne}_{\text{M}} - ^{21}\text{Ne}/^{22}\text{Ne}_{\text{A}})/f_{22} + ^{21}\text{Ne}/^{22}\text{Ne}_{\text{A}} \quad (4)$$

where f_{22} is the proportion of mantle-derived Ne in a sample, i.e.,

$$f_{22} = (^{20}\text{Ne}/^{22}\text{Ne}_{\text{M}} - ^{20}\text{Ne}/^{22}\text{Ne}_{\text{A}})/(^{20}\text{Ne}/^{22}\text{Ne}_{\text{S}} - ^{20}\text{Ne}/^{22}\text{Ne}_{\text{A}}) \quad (5)$$

and $^{20}\text{Ne}/^{22}\text{Ne}_{\text{A}}$ and $^{21}\text{Ne}/^{22}\text{Ne}_{\text{A}}$ are the isotopic ratios of air, assumed 9.8 and 0.029, respectively, $^{21}\text{Ne}/^{22}\text{Ne}_{\text{M}}$ is the measured isotopic ratio, $^{20}\text{Ne}/^{22}\text{Ne}_{\text{S}}$ is the isotopic ratio of the ‘solar’ neon component (=12.5; Trieloff et al., 2000). Selection of the solar wind value of 13.8 (Benkert et al., 1993) over the Ne-B value does not affect the general conclusions in the following discussion. As measured helium

isotope ratios are considered unmodified by air contamination, we do not apply a correction to these values.

In Fig. 15, we plot the extrapolated $^{21}\text{Ne}/^{22}\text{Ne}$ ratios for 10 Lau Basin glass samples (6 from RB; 2 from ELSC; 2 from CLSC; Table 3) against He isotopes. We show only those samples distinguishable from air Ne at the 1σ uncertainty level. We also plot He–Ne data from previous studies (6 MTJ glasses – Honda et al., 1993b; 24 xenoliths from Samoa – Poreda and Farley, 1992) after extrapolating to the mantle ratio of 12.5. Additionally, we include a series of binary mixing trajectories between postulated plume and MORB end-members. The $^{21}\text{Ne}/^{22}\text{Ne}$ of plume and MORB end-members are assumed to be 0.03118 (Trieloff and Kunz, 2005) and 0.0594, respectively. The latter is the $^{21}\text{Ne}/^{22}\text{Ne}$ ratio obtained by extrapolating the MORB trajectory to the $^{20}\text{Ne}/^{22}\text{Ne}$ of Ne-B. We adopt 90,000 (=8 R_{A}) for the $^4\text{He}/^3\text{He}$ ratio of the MORB end-member. On the other hand, there are a number of possibilities for the $^3\text{He}/^4\text{He}$ ratio of the plume end-member: 120 R_{A} (Jupiter’s atmosphere; Mahaffy et al., 1998), ~330 R_{A} (solar wind; Benkert et al., 1993), and 280–300 R_{A} (meteorites; Mazor et al., 1970; Black, 1972). We adopt the value of 280 R_{A} (Black, 1972; $^4\text{He}/^3\text{He} = 2580$) as representative of the plume end-member as it is directly associated with the Ne-B component. The curvature of the mixing curves is described by $r = ((^3\text{He}/^{22}\text{Ne})_{\text{MORB}}/(^3\text{He}/^{22}\text{Ne})_{\text{PLUME}})$, which is shown by numbers on the curves.

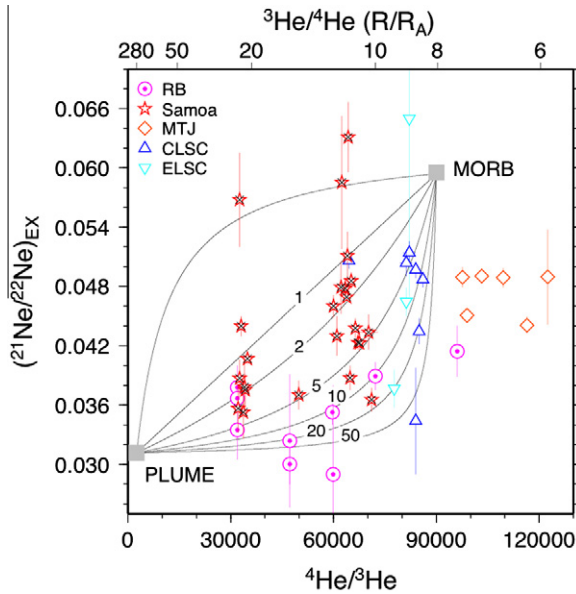


Fig. 15. $^{21}\text{Ne}/^{22}\text{Ne}_{\text{EX}}$ vs. $^4\text{He}/^3\text{He}$ ratios and binary mixing curves between a plume mantle end-member and a MORB-like component. See Section 5.5 for details.

As shown in Fig 15, the Lau Basin samples fall within three general areas of the plot. First, most of the ELSC, CLSC and RB samples fall close to plume-MORB mixing curves with r values between 5 and 20. Note that r -values greater than unity imply $(^3\text{He}/^{22}\text{Ne})_{\text{MORB}} > (^3\text{He}/^{22}\text{Ne})_{\text{PLUME}}$ and, in this respect, the Lau results are consistent with findings of OIB glasses worldwide (Hopp and Trieloff, 2008) as well as recent results for Iceland (Füri et al., 2010). Significantly, the RB samples plot closer to the plume end-member than the CLSC/ELSC samples, consistent with a greater contribution of the plume end-member in the admixture. Second, two RB samples (MGLN8-D8-3 and -D8-3b – two samples from the same dredge haul) have significantly lower r -values, ~ 2 . Therefore, if the MORB end-member $^3\text{He}/^{22}\text{Ne}$ ratio is constant throughout the Lau Basin then this high $^3\text{He}/^4\text{He}$ seamount ($22.6 R_A$) has a higher plume end-member $^3\text{He}/^{22}\text{Ne}$ ratio than others in the RB region. We note, however, that for these two RB samples the absolute value of r is highly dependent on the chosen endmember characteristics of the plume component. For example, if we chose more radiogenic and nucleogenic values for the plume end-member ($^4\text{He}/^3\text{He} \sim 20,000$ and $^{21}\text{Ne}/^{22}\text{Ne}_{\text{EX}} \sim 0.036$; Hopp and Trieloff, 2008), r can be close to 10. Finally, the MTJ samples and one RB sample (MGLN8-D14-2) fall outside the mixing boundaries defined by the series of curves between the plume and MORB end-members. For these samples, an additional end-member (with low $^3\text{He}/^4\text{He}$) is required to account for the He-Ne systematics: radiogenic He (accompanied by insignificant nucleogenic Ne) produced within the crust is the likely source of such an end-member (Section 5.1.2). Possible fractionation mechanisms are discussed below. For completeness, we include Samoa phenocrysts and xenocrysts in Fig. 15 and note that these samples have a large spread of r -values but with the majority falling between curves with r between 1 and 5. As pointed out previously (Honda

and Patterson, 1999; Hopp and Trieloff, 2008), mafic crystal phases may undergo fundamentally different trapping processes relative to basalt glasses, involving the fractionation of He with respect to Ne and Ar. Thus, we do not attempt to compare the Samoan samples with the glasses. We do note that Yamamoto et al. (2009) suggested more rapid diffusion of He to nearby magma channels as a mechanism to lower He/Ne and He/Ar in mantle xenoliths (see Fig. 16).

The fact that end-member $^3\text{He}/^{22}\text{Ne}$ compositions used in the binary mixing model above are different ($r \neq 1$) and variable ($2 < r < 20$) requires that the elemental ratio of helium to neon in one or both mantle end-members was fractionated prior to mixing (Hopp and Trieloff, 2008). We can assess whether this issue has affected the Lau Basin samples by considering the elemental ratio of ^4He to nucleogenic $^{21}\text{Ne}^*$ ($^4\text{He}/^{21}\text{Ne}^*$) and of ^3He to solar ^{22}Ne ($^3\text{He}/^{22}\text{Ne}_S$) (see discussion by Hopp and Trieloff, 2008). The ratio of primordial ^3He to solar ^{22}Ne (Graham, 2002) is given by:

$$^3\text{He}/^{22}\text{Ne}_S = \frac{(^3\text{He}/^4\text{He}_M)[^4\text{He}]_M}{[^{22}\text{Ne}]_M f_{22}} \quad (6)$$

The amount of mantle-derived nucleogenic ^{21}Ne ($^{21}\text{Ne}^*$) in a sample is given by:

$$^{21}\text{Ne}^* = ^{22}\text{Ne}_S (^{21}\text{Ne}/^{22}\text{Ne}_{\text{EX}} - ^{21}\text{Ne}/^{22}\text{Ne}_S) \quad (7)$$

Here, we use the isotope composition of Ne-B as the value for ‘solar’ mantle neon in order to calculate $^3\text{He}/^{22}\text{Ne}_S$ and $^4\text{He}/^{21}\text{Ne}^*$.

Fig. 16 shows a plot of $^3\text{He}/^{22}\text{Ne}_S$ vs. $^4\text{He}/^{21}\text{Ne}^*$ for the Lau Basin samples of this study. Also plotted for comparison are glass data for Iceland, Loihi Seamount, the Manus Basin and MORB (see Füri et al., 2010 and references therein; Shaw et al., 2001 for the Manus Basin data). As shown in the figure, OIB-like samples (Iceland and Loihi)

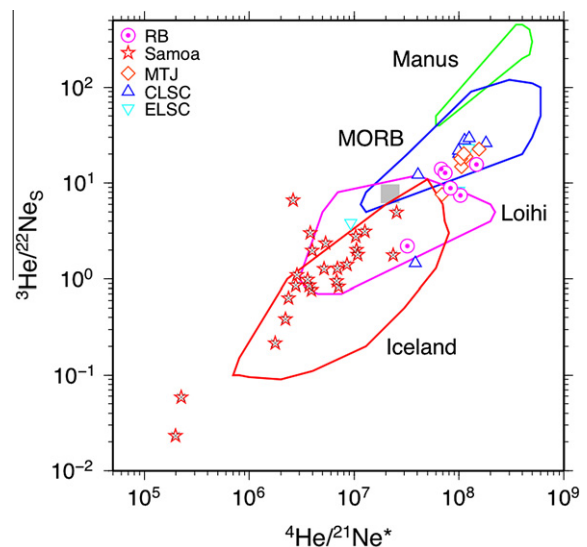


Fig. 16. $^3\text{He}/^{22}\text{Ne}_S$ vs. $^4\text{He}/^{21}\text{Ne}^*$ for the Lau Basin samples. Also shown are fields for OIB- (Iceland and Loihi), MORB-like samples (Füri et al., 2010 and references therein) and a back-arc basin (Manus Basin; Shaw et al., 2001). The gray square shows the values for the Earth's mantle ($^3\text{He}/^{22}\text{Ne}_S = 7.7$, Honda and McDougall, 1998; $^4\text{He}/^{21}\text{Ne}^* = 2.2 \times 10^7$, Yatsevich and Honda, 1997).

have distinctively lower He/Ne ratios than that postulated for the Earth's mantle (primordial $^3\text{He}/^{22}\text{Ne}_S = 7.7$, Honda and McDougall, 1998; radiogenic/nucleogenic production ratio $^4\text{He}/^{21}\text{Ne}^* = 2.2 \times 10^7$, Yatsevich and Honda, 1997). As discussed by Hopp and Trieloff (2008), OIB have low He/Ne ratios because of a 'helium deficit' which could have resulted from the more compatible behavior of He relative to Ne (and Ar) during partial melting. In this way, a small-degree rising plume melt – deficient in He – mixes with shallow large-degree MORB melt which shows no such deficit to produce the range of observed He–Ne isotopes compositions in OIB. The elevated He/Ne and He/Ar ratios of MORBs can be attributed to vesiculation and vesicle loss (Sarda and Moreira, 2002) – although refer to Honda and Patterson (1999) for an alternative hypothesis. Compared to OIB magma, MORB magma undergoes more extensive vesicle loss that enables preferential loss of Ne and Ar relative to He due to their lower solubilities in magma. In either case, the linear correlation of $^3\text{He}/^{22}\text{Ne}_S$ vs. $^4\text{He}/^{21}\text{Ne}^*$ of all sample suites, including the Lau Basin, with a slope ~ 1 implies that any He–Ne fractionation must have occurred relatively recently in order to preserve $^4\text{He}/^{21}\text{Ne}^*$ ratios different from the production ratio (Honda and Patterson, 1999). In turn, this observation restricts the fractionation event and subsequent mixing between end-members to the relatively shallow mantle and/or site where the lavas are erupted.

A remarkable feature of the Lau Basin dataset is the fact that most samples – from the RB, ELSC/CLSC and MTJ – have He/Ne ratios higher than the Earth's mantle, consistent with observations made previously for the Lau Basin (Honda et al., 1993b; Honda and Patterson, 1999). In contrast, high $^3\text{He}/^4\text{He}$ ratio samples from Samoa have low He/Ne ratios, overlapping with Iceland and Loihi Seamount (Fig. 16). In this respect, it is somewhat surprising that the RB samples with OIB-like high $^3\text{He}/^4\text{He}$ ratios ($>10 R_A$) have He/Ne elemental ratios which do not overlap with Samoa and other OIB localities that possess similarly high $^3\text{He}/^4\text{He}$ values. Interestingly, the one other locality that shares the characteristics of high $^3\text{He}/^4\text{He}$ and high He/Ne elemental ratios with the RB region of the Lau Basin is submarine spreading centers in the Manus back-arc basin. The first-order implication of this observation is that if the helium enrichment hypothesis of Honda and Patterson (1999) is valid then the process is unique to rifting regions at mid-ocean ridges, and back arc basins, particularly where subduction components are present.

Thus, the combined He–Ne systematics allow us to invoke a binary mantle mixture scenario involving plume-like and MORB-like end-member compositions to account for the majority of samples erupted in the Lau Basin – but with an additional crustal volatile component needed in some cases, particularly in the MTJ. The plume-like component is most prevalent in the RB and is likely variably fractionated in its elemental He/Ne ratio. Such a fractionation occurred relatively recently but prior to mixing with ambient MORB-like mantle. High He/Ne ratios observed in the RB region of the Lau Basin are found at mid-ocean ridges and at one other back-arc basin only. This observation may be indicative of a He–Ne fractionation mechanism operating exclusively at oceanic rifting environments.

6. SUMMARY AND CONCLUDING REMARKS

This study of volatiles captured in quenched volcanic glasses from various regions of the Lau back-arc basin has revealed significant heterogeneity in both the abundance and isotope characteristics of various species. Helium isotopes vary widely throughout the basin with the highest values ($>\text{MORB-type He}$) occurring as far north as the RR, throughout the RB and as far south as the PR. MORB-like He ($8 \pm 1 R_A$) characterizes the all other areas of the Lau Basin (NV, MTJ, CLSC, ELSC) but some samples – particularly lavas that show evidence of differentiation and/or crustal contamination – have lower, more radiogenic, values. Addition of radiogenic He is predominant in samples erupted along the VFR. Air additions of Ne and Ar are found in all samples but two trends emerge in 3-isotope Ne space. Samples from the CLSC and ELSC have MORB-like Ne trajectories indicating close coupling between He and Ne isotope systematics in this part of the basin. In contrast, RB samples show higher $^{20}\text{Ne}/^{22}\text{Ne}$ ratios for a given $^{21}\text{Ne}/^{22}\text{Ne}$, consistent with a greater proportion of solar-derived Ne in the source. High elemental He/Ne ratios ($^3\text{He}/^{22}\text{Ne}_S$ and $^4\text{He}/^{21}\text{Ne}^*$) are observed throughout the Lau Basin but the RB, and only one other region worldwide, has both high He/Ne and $^3\text{He}/^4\text{He}$.

The CO_2 inventory of Lau Basin glasses is dominated by CO_2 dissolved in the glass phase with a relatively small proportion of the CO_2 captured by vesicles. The highest CO_2 concentrations (>100 ppm) are found in the CLSC, ELSC and PR with lower concentrations tending to characterize samples erupted at shallower water depths (RB). Water concentrations vary regionally throughout the basin. The lowest concentrations (<0.5 wt%) characterize the CLSC, ELSC and PR whereas the MTJ has the highest (up to ~ 2 wt%). RB samples have intermediate values of water. Similar patterns are observed for F, Cl and S.

There are a number of controls on the chemistry of the Lau Basin samples: mantle source variation and source mixing, fractional crystallization and crustal contamination processes. The volatile chemistry reflects all three processes with the major shallow mechanisms being magmatic degassing and additions of extraneous volatiles (from air, seawater and/or crustal contamination) which act to mask intrinsic mantle source characteristics. Combining constraints imposed by CO_2 - $\delta^{13}\text{C}$ variations, it is possible to reconstruct primary CO_2 contents prior to degassing. Primary CO_2 concentrations estimated for RB melts ($\sim 940 \pm 170$ ppm) are higher than those of the CLSC/ELSC ($\sim 640 \pm 120$ ppm) as is their primary $\delta^{13}\text{C}$ composition. Both observations are consistent with observations in other hotspot-related magmas compared to MORB melts. However, there is no discernible difference in primary CO_2/Nb ratios between mantle characterized by high $^3\text{He}/^4\text{He}$ (RB) and MORB-like He isotope ratios (ELSC/CLSC). Reconstructed values of primary CO_2/Nb in the Lau Basin contribute to a growing body of evidence that mantle sources are more heterogeneous in this parameter than initially envisaged. In contrast, reconstructed He/Ne elemental ratios are high throughout the Lau Basin, even in the high $^3\text{He}/^4\text{He}$ RB region: this observation identifies

the Lau Basin mantle source as one of only two high $^3\text{He}/^4\text{He}$ regions worldwide with evidence of extensive enrichment of mantle He relative to Ne.

ACKNOWLEDGMENTS

This work was funded by NSF Grant OCE-0453608. Hahm was partially supported by the Korea Polar Research Institute (PP09040). We acknowledge an award from the University of California Ship Funds for support of the Magellan expedition – Leg 8. Aaron Pietruszka and Evelyn Füri are thanked for help during sea-going operations. Martin Wahlen kindly allowed access to stable isotope facilities and Liyan Tian contributed some of the chemical analyses. Comments and suggestions by Pete Burnard, Jens Hopp, Phillip Sarda and one anonymous reviewer are gratefully acknowledged.

APPENDIX A. PETROLOGY OF THE LAU BASIN

There is an extensive database offering insight into the petrology of lavas in the Lau Basin (e.g., Hawkins, 1974, 1989; Hawkins and Melchior, 1985; Jenner et al., 1987; Boespflug et al., 1990; Sunkel, 1990; Vallier et al., 1991; Falloon et al., 1994; Pearce et al., 1995; Tian et al., 2008; Escrig et al., 2009).

A.1. Central Lau Basin (CLSC, ELSC and Relay Zone (RZ))

The central Lau Basin lavas consist mainly of mid-ocean ridge basalt (MORB)-like tholeiitic basalts (e.g., Bryan et al., 1976; Viereck et al., 1989; Tian et al., 2008; Escrig et al., 2009). Lavas from ELSC, CLSC, and RZ range from relatively primitive (up to 8% MgO, Mg# 64) to moderately fractionated (4–5% MgO, Mg# 43–50). There are other slight differences in major element contents: compared to CLSC basalts with similar MgO contents, ELSC and RZ basalts have higher SiO_2 and Al_2O_3 and lower FeO^* , Na_2O and TiO_2 . In terms of rare earth elements, the Central Lau Basin lavas are MORB-like: however, they are enriched in large-ion lithophile element (LILE; e.g., Rb, Ba and K) – up to 10 times compared to normal-MORB, and are variably depleted in high field-strength elements (HFSE; e.g., Nb and Ta). They have $^{143}\text{Nd}/^{144}\text{Nd}$ similar to Indian MORB, although generally with higher $^{87}\text{Sr}/^{86}\text{Sr}$ for given $^{143}\text{Nd}/^{144}\text{Nd}$ relative to Indian MORB. In comparison, ELSC and RZ show more distinctive negative Nb and Ta anomalies (Tian et al., 2008; Escrig et al., 2009). Additionally, ELSC and RZ lavas have lower $^{143}\text{Nd}/^{144}\text{Nd}$ than CLSC for given range of $^{87}\text{Sr}/^{86}\text{Sr}$ values (Tian et al., 2008).

A.2. Mangatolu Triple Junction

Samples from the MTJ include basalts, basaltic andesites and andesites. These rocks share many of the characteristics of the VFR samples in terms of major and trace elements, but in general are much more like the ELSC–CLSC lavas than those of the Tofua Arc. A possible reason for the minimal arc signature in MTJ lavas, despite their

location, is that the original “arc component” in the supra-subduction zone (SSZ) mantle wedge has long since been stripped out and replaced by MORB-source mantle. Spreading rates are relatively fast, ~ 90 mm/yr (Zellmer and Taylor, 2001).

A.3. Peggy Ridge

The morphology of PR and the variety of dredged rock types from it suggest that the PR is comprised of uptilted blocks of old crust. The westernmost end has transitional basalt, although one site on the western part of the ridge has yielded primitive, highly depleted basalt having many characteristics of basaltic komatiite or boninite (Hawkins and Melchior, 1985). These rocks resemble early-formed melts in many SSZ settings and may represent the first magmas erupted as the Lau Basin opened. The middle and eastern parts of the PR are composed of fractionated MORB-like basalt with relatively high TiO_2 (e.g., 2%), FeO^* (e.g., 11–12%), and Na_2O (e.g., 3%) (Hawkins and Melchior, 1985).

A.4. Seamounts

North and east of the PR are a number of young, volcanically active seamounts. Rochambeau Bank has rocks relatively more enriched in alkalis and HFSE than most other Lau Basin lavas and quite different from samples of the NLSC (which extends toward the RB). In some respects it is arc-like, but its enrichment in HFSE and Sr and Nd isotopic signature suggest an ocean island basalt (OIB) or enriched-MORB affinity. Poreda (1985) and Poreda and Craig (1992) reported $^3\text{He}/^4\text{He}$ of 11.0 and 14.1 R_A ($R_A = \text{air } ^3\text{He}/^4\text{He}$) for RB samples and a ratio of 22.0 R_A for a sample from the nearby seafloor. They proposed that these elevated $^3\text{He}/^4\text{He}$ ratios represent contributions from a Samoan plume component that has been entrained under the northern Lau Basin. These high $^3\text{He}/^4\text{He}$ ratios were confirmed recently by Lupton et al. (2009). Niufo’ou Island has moderately fractionated basalts with 49–50% SiO_2 , 5.1–7.2% MgO, and 1.4–1.8% TiO_2 (Reay et al., 1974). The Ni content is low (34–60 ppm) for this MgO range, as is Ba (35–68 ppm). Strontium, Nd, and Pb isotope data all show that NV lavas differ from Tofua Arc samples. Ewart and Hawkesworth (1987) concluded that NV lavas are derived from a distinct magma source with an OIB signature in spite of their general chemical similarity to MORB. Poreda and Craig (1992) showed that gases collected in the crater lake, Vai Kona, on NV have MORB-like $^3\text{He}/^4\text{He}$ ratios of 7.8 R_A .

A.5. The Valu Fa Ridge

The VFR at the southern tip of the ELSC (south of $21^\circ 20'S$) has an extensive hydrothermal field underlain by a small axial magma chamber (Morton and Sleep, 1985). It is capped with “oceanic andesite” that has chemical and isotopic signatures resembling those for lavas from the nearby Tofua Arc (Vallier et al., 1991). The main rock types recovered from the VFR are highly vesicular,

glass-rich low-K andesites with 54–60% SiO₂, 0.36–0.57% K₂O (Davis et al., 1990; Vallier et al., 1991). However, Sunkel (1990) reported recovery of three samples of high silica dacitic glasses (66–70% SiO₂, 0.62–0.87% K₂O) and Davis et al. (1990) described moderately fractionated basalt (5.7–6.1% MgO). The VFR is propagating southward into older crust of uncertain composition, but this crust may be equivalent to the rifted forearc terrane that forms the basin and range-type seafloor of the western Lau Basin. Rocks from near the propagating rift tip include some low-K, high silica andesites that are probably extreme fractionates formed as the rift penetrated older, cold crust.

APPENDIX B. CALCULATIONS OF CO₂ IN PRE-ERUPTIVE MELTS

	C ¹ (RNDB15-5-8)	C ² (RNDB15-35-1)	C _p	d _p
d _r (‰)	−8.4	−8.5	638.3 ^c	−6.69 ^d
C _{rBED} (ppm)	171.9	144.5		−6.69 ^e
C _{rFED} (ppm)	288.6 ^a	276.5 ^b		−6.55 ^f −6.55 ^g

^aCalculated from d_r¹ and the regression line (FED trajectory).

^bCalculated from d_r² and the regression line (FED trajectory).

^cCalculated from Eq. (3).

^dCalculated from Eq. (1) using d_r¹ and C_{rBED}¹.

^eCalculated from Eq. (1) using d_r² and C_{rBED}².

^fCalculated from Eq. (1) using d_r¹ and C_{rBED}¹.

^gCalculated from Eq. (1) using d_r² and C_{rBED}².

REFERENCES

- Aubaud C., Pineau F., Jambon A. and Javoy M. (2004) Kinetic disequilibrium of C, He, Ar and carbon isotopes during degassing of mid-ocean ridge basalts. *Earth Planet. Sci. Lett.* **222**, 391–406.
- Bach W. and Niedermann S. (1998) Atmospheric noble gases in volcanic glasses from the southern Lau Basin: origin from the subducting slab? *Earth Planet. Sci. Lett.* **160**, 297–309.
- Baker E., Resing J., Walker S., Martinez F., Taylor B. and Nakamura K. (2006) Abundant hydrothermal venting along melt-rich and melt-free ridge segments in the Lau back-arc basin. *Geophys. Res. Lett.* **33**. ARTN L07308.
- Ballentine C. J. and Barfod D. N. (2000) The origin of air-like noble gases in MORB and OIB. *Earth Planet. Sci. Lett.* **180**, 39–48.
- Benkert J.-P., Baur H., Signer P. and Wieler R. (1993) He, Ne, and Ar from the solar wind and solar energetic particles in lunar ilmenites and pyroxenes. *J. Geophys. Res.* **98**, 13147–13162.
- Bezos A., Escrig S., Langmuir C. H., Michael P. J. and Asimow P. D. (2009) Origins of chemical diversity of back-arc basin basalts: a segment-scale study of the Eastern Lau Spreading Center. *J. Geophys. Res.* **114**, B06212. doi:10.1029/2008JB005924.
- Black D. C. (1972) On the origins of trapped helium, neon and argon isotopic variations in meteorites: I. Gas-rich meteorites, lunar soil and breccia. *Geochim. Cosmochim. Acta* **36**, 347–375.
- Boespflug X., Dosso L., Bougault H. and Joron J. L. (1990) Trace element and isotopic (Sr, Nd) geochemistry of volcanic rocks from the Lau Basin. *Geol. Jahrb.* **92**, 503–516.
- Brenan J. M., Shaw H. F., Ryerson F. J. and Phinney D. L. (1995) Mineralaqueous fluid partitioning of trace-elements at 900 °C and 2.0 GPa – constraints on the trace-element chemistry of mantle and deep-crustal fluids. *Geochim. Cosmochim. Acta* **59**, 3331–3350.
- Bryan W. B., Thompson G., Frey F. A. and Dickey J. S. (1976) Inferred geologic settings and differentiation in basalts from the Deep Sea Drilling Project. *J. Geophys. Res.* **81**, 4285–4304.
- Burnham C. W. (1979) Magmas and hydrothermal fluids. In *Geochemistry of Hydrothermal Ore Deposits* (ed. H. Barnes). John Wiley and Sons, Inc., pp. 71–136.
- Cartigny P., Jendrzewski N., Pineau F., Petit E. and Javoy M. (2001) Volatile (C, N, Ar) variability in MORB and the respective roles of mantle source heterogeneity and degassing: the case of the Southwest Indian Ridge. *Earth Planet. Sci. Lett.* **194**, 241–257.
- Cartigny P., Pineau F., Aubaud C. and Javoy M. (2008) Towards a consistent mantle carbon flux estimate: insights from volatile systematics (H₂O/Ce, δD, CO₂/Nb) in the North Atlantic mantle (140°N and 340°N). *Earth Planet. Sci. Lett.* **265**, 672–685.
- Cole J. W., Gill J. B. and Woodhall D. (1985) Petrologic history of the Lau Ridge, Fiji. In *Geology and Offshore Resources of Pacific Island Arcs – Tonga Region* (eds. D. Scholl and T. Vallier). Circum-Pacific Council for Energy and Mineral Resources, pp. 373–414.
- Craig H., Marti K. and Wiens R. (1993) A static mass spectrometer with triple collection for nitrogen and neon isotopes. *Oceanography Reference Series* 93-11, Scripps Institution of Oceanography.
- Davis A. S., Clague D. A. and Morton J. L. (1990) Volcanic glass compositions from two spreading centers in Lau Basin, South West Pacific Ocean. *Geol. Jahrb.* **92**, 481–501.
- Des Marais D. J. (1978) Variable-temperature cryogenic trap for the separation of gas mixtures. *Anal. Chem.* **50**, 1405–1406.
- Dixon J. E., Clague D. A., Wallace P. and Poreda R. J. (1997) Volatiles in alkalic basalts from the North Arch Volcanic Field, Hawaii: extensive degassing of deep submarine-erupted alkalic series lavas. *J. Petrol.* **38**, 911–939.
- Dixon J. E., Stolper E. M. and Holloway J. R. (1995) An experimental study of water and carbon dioxide solubilities in mid-ocean ridge basaltic liquids: Part I. Calibration and solubility models. *J. Petrol.* **36**, 1607–1631.
- Dixon J. E., Stolper E. M. and Delaney J. R. (1988) Infrared spectroscopic measurements of CO₂ and H₂O in Juan de Fuca Ridge basaltic glasses. *Earth Planet. Sci. Lett.* **90**, 87–104.
- Escrig S., Bezos A., Goldstein S. L., Langmuir C. H. and Michael P. J. (2009) Mantle source variations beneath the Eastern Lau Spreading Center and the nature of subduction components in the Lau Basin–Tonga arc system. *Geochem. Geophys. Geosyst.* **10**, Q040414. doi:10.1029/2008GC002281.
- Ewart A. and Hawkesworth C. J. (1987) The Pleistocene–Recent Tonga–Kermadec arc lavas: interpretation of new isotopic and rare earth data in terms of a depleted mantle source model. *J. Petrol.* **28**, 495–530.
- Exley R. A., Matthey D. P., Clague D. A. and Pillinger C. T. (1986) Carbon isotope systematic of a mantle hotspot: A comparison of Loihi seamount and MORB glasses. *Earth Planet. Sci. Lett.* **78**, 189–199.
- Falloon T. J., Green D. H. and Jaques A. L. (1994) Refractory magmas in back-arc basin settings: experimental constraints on a Lau Basin example. *Mineral. Mag.* **58**, 263–264.
- Farley K. A. and Craig H. (1994) Atmospheric argon contamination of ocean island basalt olivine phenocrysts. *Geochim. Cosmochim. Acta* **58**, 2509–2517.

- Fine G. J. and Stolper E. M. (1986) Dissolved carbon dioxide in basaltic glasses: concentrations and speciation. *Earth Planet. Sci. Lett.* **76**, 263–278.
- Füri E., Hilton D. R., Halldorsson S. A., Barry P. H., Hahm D., Fischer T. P. and Gronvold K. (2010) Apparent decoupling of the He and Ne isotope systematics of the Icelandic mantle: the role of He depletion, melt mixing, degassing fractionation and air interaction. *Geochim. Cosmochim. Acta* **74**, 3307–3332.
- Gerlach T. M. and Graeber E. J. (1985) Volatile budget of Kilauea volcano. *Nature* **313**, 273–277.
- Gill J. B. (1976) Composition and age of Lau Basin and ridge volcanic rocks: implications for evolution of an interarc basin and remnant arc. *Bull. Geol. Soc. Am.* **87**, 1384–1395.
- Graham D. W. (2002) Noble gas isotope geochemistry of mid-ocean ridge and ocean island basalts: characterization of mantle source reservoirs. *Rev. Mineral. Geochem.* **47**, 247–315.
- Greenland L. P., Rose W. I. and Stokes J. B. (1985) An estimate of gas emissions and magmatic gas content from Kilauea volcano. *Geochim. Cosmochim. Acta* **49**, 125–129.
- Harris D. (1981) The concentration of CO₂ in submarine tholeiitic basalts. *J. Geol.* **89**, 689–701.
- Hauri E. (2002) SIMS analysis of volatiles in silicate glasses: 2. Isotopes and abundances in Hawaiian melt inclusions. *Chem. Geol.* **183**, 115–141.
- Hawkins J. W. (1974) Geology of the Lau Basin, a marginal sea behind the Tonga Arc. In *The Geology of Continental Margins*. Springer-Verlag, New York, pp. 505–520.
- Hawkins J. W. (1988) Cruise Report – PAPATUA Expedition, Leg 04, R/V Thomas Washington. SIO Reference Series 88-14, Scripps Institution of Oceanography.
- Hawkins J. W. (1989) Cruise Report Roundabout Expedition Leg 14, 23 Jan 89 to 1 Feb 89, Suva, Fiji to Nuku'alofa, Tonga, Leg 15, 2 Feb 89 to 3 Mar 89, Nuku'alofa, Tonga to Pago Pago, American Samoa, R/V Thomas Washington. Technical Report, Scripps Institution of Oceanography.
- Hawkins J. W. and Melchior J. T. (1985) Petrology of Mariana Trough and Lau Basin basalts. *J. Geophys. Res.* **90**, 431–468.
- Hilton D. R. (1996) The helium and carbon isotope systematics of a continental geothermal system: results from monitoring studies at Long Valley caldera (California, USA). *Chem. Geol.* **127**, 269–295.
- Hilton D. R., Gronvold K., Sveinbjornsdottir A. E. and Hammerschmidt K. (1998) Helium isotope evidence for off-axis degassing of the Icelandic hotspot. *Chem. Geol.* **149**, 173–187.
- Hilton D. R., Hammerschmidt K., Loock G. and Frierichsen H. (1993) Helium and argon isotope systematics of the central Lau Basin and Valu Fa Ridge: evidence of crust/mantle interactions in a back-arc basin. *Geochim. Cosmochim. Acta* **57**, 2819–2841.
- Hofmann A. W. (1988) Chemical differentiation of the earth: the relationship between mantle, continental crust, and oceanic crust. *Earth Planet. Sci. Lett.* **90**, 297–314.
- Honda M., McDougall I. and Patterson D. B. (1993a) Solar noble gases in the earth: the systematics of helium–neon isotopes in mantle derived samples. *Lithos* **30**, 257–265.
- Honda M., McDougall I., Patterson D. B., Dougeris A. and Clague D. A. (1991) Possible solar noble-gas component in Hawaiian basalts. *Nature* **349**, 149–151.
- Honda M. and McDougall I. (1998) Primordial helium and neon in the earth – a speculation on early degassing. *Geophys. Res. Lett.* **25**, 1951–1954.
- Honda M., Patterson D. B., McDougall I. and Falloon T. J. (1993b) Noble gases in submarine pillow basalt glasses from the Lau Basin: detection of a solar component in backarc basin basalts. *Earth Planet. Sci. Lett.* **120**, 135–148.
- Honda M. and Patterson D. B. (1999) Systematic elemental fractionation of mantle-derived helium, neon, and argon in mid-oceanic ridge glasses. *Geochim. Cosmochim. Acta* **63**, 2863–2874.
- Hopp J. and Trieloff M. (2008) Helium deficit in high-³He/⁴He parent magmas: predegassing fractionation, not a “helium paradox”. *Geochem. Geophys. Geosyst.* **9**, Q03009. doi:10.1029/2007GC001833.
- Jackson M. G., Kurz M. D., Hart S. R. and Workman R. K. (2007) New Samoan lavas from Ofu Island reveal a hemispherically heterogeneous high ³He/⁴He mantle. *Earth Planet. Sci. Lett.* **264**, 360–374.
- Jacobs A. M., Harding A. J. and Kent G. M. (2007) Axial crustal structure of the Lau back-arc basin from velocity modeling of multichannel seismic data. *Earth Planet. Sci. Lett.* **259**, 239–255.
- Jambon A., Weber H. and Braun O. (1986) Solubility of He, Ne, Ar, Kr and Xe in a basalt melt in the range 1250–1600 °C. Geochemical implications. *Geochim. Cosmochim. Acta* **50**, 401–408.
- Jambon A. and Zimmermann J. L. (1990) Water in oceanic basalts: evidence for dehydration of recycled crust. *Earth Planet. Sci. Lett.* **101**, 323–331.
- Javoy M. and Pineau F. (1991) The volatiles record of a popping rock from the Mid-Atlantic Ridge at 14°N – chemical and isotopic composition of gas trapped in the vesicles. *Earth Planet. Sci. Lett.* **107**, 598–611.
- Javoy M., Pineau F. and Iiyama I. (1978) Experimental-determination of isotopic fractionation between gaseous CO₂ and carbon dissolved in tholeiitic magma tholeiitic magma – preliminary study. *Contrib. Mineral. Petrol.* **67**, 35–39.
- Jenner G. A., Cawood P. A., Rautenschlein M. and White W. M. (1987) Composition of back-arc basin volcanics, Valu Fa Ridge, Lau Basin: evidence for a slab-derived component in their mantle source. *J. Volcanol. Geotherm. Res.* **32**, 209–222.
- Kent A. J. R., Norman M. D., Hutcheon I. D. and Stolper E. M. (1999) Assimilation of seawater-derived components in an oceanic volcano: evidence from matrix glasses and glass inclusions from Loihi seamount, Hawaii. *Chem. Geol.* **156**, 299–319.
- Kent A. J. R., Peate D. W., Newman S., Stolper E. M. and Pearce J. A. (2002) Chlorine in submarine glasses from the Lau Basin: seawater contamination and constraints on the composition of slab-derived fluids. *Earth Planet. Sci. Lett.* **6315**, 361–377.
- Koleszar A. M., Saal A. E., Hauri E. H., Nagle A. N., Liang Y. and Kurz M. D. (2009) The volatile contents of the Galapagos plume: evidence for H₂O and F open system behavior in melt inclusions. *Earth Planet. Sci. Lett.* **287**, 442–452. doi:10.1016/j.epsl.2009.08.029.
- Lupton J. E., Arculus R. J., Greene R. R., Evans L. J. and Goddard C. I. (2009) Helium isotope variations in seafloor basalts from the Northwest Lau Backarc Basin: mapping the influence of the Samoan hotspot. *Geophys. Res. Lett.* **36**, L17313.
- Macpherson C. G., Hilton D. R. and Hammerschmidt K. (2010) No slab-derived CO₂ in Mariana Trough back-arc basalts: implications for carbon subduction and for temporary storage of CO₂ beneath slow spreading ridges. *Geochem. Geophys. Geosyst.* **11**, Q11007. doi:10.1029/2010GC003293.
- Macpherson C. G., Hilton D. R., Mertz D. F. and Dunai T. J. (2005) Sources, degassing, and contamination of CO₂, H₂O, He, Ne, and Ar in basaltic glasses from Kolbeinsey Ridge, North Atlantic. *Geochim. Cosmochim. Acta* **69**, 5729–5746.
- Macpherson C. G., Hilton D. R., Newman S. and Matthey D. P. (1999) CO₂, ¹³C/¹²C and H₂O variability in natural basaltic glasses: a study comparing stepped heating and FTIR spectroscopic techniques. *Geochim. Cosmochim. Acta* **63**, 1805–1813.

- Macpherson C. G. and Matthey D. P. (1994) Carbon isotope variations of CO₂ in Central Lau Basin basalts and ferrobasalts. *Earth Planet. Sci. Lett.* **121**, 263–276.
- Mahaffy P. R., Donahue T. M., Atreya S. K., Owen T. C. and Niemann H. B. (1998) Galileo probe measurements of D/H and ³He/⁴He in Jupiter's atmosphere. *Space Sci. Rev.* **84**, 251–263.
- Marty B. and Zimmermann L. (1999) Volatiles (He, C, N, Ar) in mid-ocean ridge basalts: assessment of shallow-level fractionation and characterization of source composition. *Geochim. Cosmochim. Acta* **63**, 3619–3633.
- Matthey D. P. (1991) Carbon-dioxide solubility and carbon isotope fractionation in basaltic melt. *Geochim. Cosmochim. Acta* **55**, 3467–3473.
- Matthey D. P., Carr R. H., Wright I. P. and Pillinger C. T. (1984) Carbon isotopes in submarine basalts. *Earth Planet. Sci. Lett.* **70**, 196–206.
- Mazor E., Heymann D. and Anders E. (1970) Noble gases in carbonaceous chondrites. *Geochim. Cosmochim. Acta* **34**, 781–824.
- Moreira M., Kunz J. and Allegre C. (1998) Rare gas systematics in popping rock: isotopic and elemental compositions in the upper mantle. *Science* **279**, 1178–1181.
- Morton J. L. and Sleep N. H. (1985) A mid-ocean ridge thermal model: constraints on the volume of axial hydrothermal heat flux. *J. Geophys. Res.* **90**, 11–345.
- Moune S., Sigmarsson O., Thordarson T. and Gauthier P.-J. (2007) Recent volatile evolution in the magmatic system of Hekla volcano, Iceland. *Earth Planet. Sci. Lett.* **255**, 373–389. doi:10.1016/j.epsl.2006.12.024.
- Newman S. and Lowenstern J. B. (2002) VolatileCalc: a silicate melt–H₂O–CO₂ solution model written in Visual Basic for Excel. *Comput. Geosci.* **28**, 597–604.
- Newman S., Stolper E. M. and Stern R. (2000) H₂O and CO₂ in magmas from the Mariana arc and back arc systems. *Geochem. Geophys. Geosyst.* **1**, 1–38.
- Niedermann S., Graf T. and Marti K. (1993) Mass spectrometric identification of cosmic-ray-produced neon in terrestrial rocks with multiple neon components. *Earth Planet. Sci. Lett.* **118**, 65–73.
- Ozima M. and Podosek F. (2002) *Noble Gas Geochemistry*. Cambridge University Press.
- Parson L. M. and Hawkins J. W. (1994) Two-stage ridge propagation and the geological history of the Lau backarc basin. In *Proceedings of the Ocean Drilling Program. Scientific Results*, vol. 135, pp. 819–828.
- Pearce J. A., Ernewein M., Bloomer S. H., Parson L. M., Murton B. J. and Johnson L. E. (1995) Geochemistry of Lau Basin volcanic rocks: influence of ridge segmentation and arc proximity. In *Volcanism Associated with Extension at Consuming Plate Margins* (ed. J. Smellie). Geol. Soc. London Special Paper 81, London, pp. 53–75.
- Pearce J. A., Kempton P. D. and Gill J. B. (2007) Hf–Nd evidence for the origin and distribution of mantle domains in the SW Pacific. *Earth Planet. Sci. Lett.* **260**, 98–114.
- Pineau F. and Javoy M. (1983) Carbon isotopes and concentrations in mid-oceanic ridge basalts. *Earth Planet. Sci. Lett.* **62**, 239–257.
- Poreda R. J. (1985) Helium-3 and deuterium in back-arc basalts – Lau Basin and the Mariana Trough. *Earth Planet. Sci. Lett.* **73**, 244–254.
- Poreda R. J. and Craig H. (1992) He and Sr isotopes in the Lau Basin mantle: depleted and primitive mantle components. *Earth Planet. Sci. Lett.* **113**, 487–493.
- Poreda R. J. and Farley K. A. (1992) Rare gases in Samoan xenoliths. *Earth Planet. Sci. Lett.* **113**, 129–144.
- Reay A., Rooke J. M., Wallace R. C. and Whelan P. (1974) Lavas from Niuafu'ou Island, Tonga, resemble ocean-floor basalts. *Geology* **2**, 605–606.
- Saal A. E., Hauri E. H., Langmuir C. H. and Perfit M. R. (2002) Vapour undersaturation in primitive mid-ocean-ridge basalt and the volatile content of earth's upper mantle. *Nature* **419**, 451–455.
- Sano Y. and Marty B. (1995) Origin of carbon in fumarolic gas from island arcs. *Chem. Geol.* **119**, 265–274.
- Sarda P. (2004) Surface noble gas recycling to the terrestrial mantle. *Earth Planet. Sci. Lett.* **228**, 49–63. doi:10.1016/j.epsl.2004.09.026.
- Sarda P. and Moreira M. (2002) Vesiculation and vesicle loss in mid-ocean ridge basalt glasses: He, Ne, Ar elemental fractionation and pressure influence. *Geochim. Cosmochim. Acta* **66**, 1449–1458.
- Sarda P., Staudacher T. and Allègre C. (1988) Neon isotopes in submarine basalts. *Earth Planet. Sci. Lett.* **91**, 73–88.
- Scarsi P. (2000) Fractional extraction of helium by crushing of olivine and clinopyroxene phenocrysts: effects on the ³He/⁴He measured ratio. *Geochim. Cosmochim. Acta* **64**, 3751–3762.
- Shaw A. M., Behn M. D., Humphris S. E., Sohn R. A. and Gregg P. M. (2010) Deep pooling of low degree melts and volatile fluxes at the 85°E segment of the Gakkel Ridge: evidence from olivine-hosted melt inclusions and glasses. *Earth Planet. Sci. Lett.* **289**, 311–322. doi:10.1016/j.epsl.2009.11.018.
- Shaw A. M., Hilton D. R., Macpherson C. G. and Sinton J. M. (2001) Nucleogenic neon in high ³He/⁴He lavas from the Manus back-arc basin: a new perspective on He–Ne decoupling. *Earth Planet. Sci. Lett.* **194**, 53–66.
- Shaw A. M., Hilton D. R., Macpherson C. G. and Sinton J. M. (2004) The CO₂–He–Ar–H₂O systematics of the Manus back-arc basin: resolving source composition from degassing and contamination effects. *Geochim. Cosmochim. Acta* **68**, 1837–1856.
- Smith G. P., Wiens D. A., Fischer K. M., Dorman L. M., Webb S. C. and Hildebrand J. A. (2001) A complex pattern of mantle flow in the Lau backarc. *Science* **292**, 713–716.
- Stecher O. (1998) Fluorine geochemistry in volcanic rock series: examples from Iceland and Jan Mayen – evidence for mantle heterogeneity beneath Iceland. *Geochim. Cosmochim. Acta* **62**, 3117–3130.
- Sunkel G. (1990) Petrology and geochemistry of submarine lavas from the Lau Basin (SW, Pacific). *Mar. Min.* **9**, 205–234.
- Tian L., Castillo P. R., Hawkins J. W., Hilton D. R., Hannan B. B. and Pietruszka A. J. (2008) Major and trace element and Sr–Nd isotope signatures of lavas from the Central Lau Basin: implications for the nature and influence of subduction components in the back-arc mantle. *J. Volcanol. Geotherm. Res.* **178**, 657–670.
- Tian L. (2011) Petrogenesis of intraplate lavas from isolated volcanoes in the Pacific: implications for the origin of the enriched mantle source of OIB. Ph.D. thesis, University of California, San Diego.
- Trieloff M. and Kunz J. (2005) Isotope systematics of noble gases in the Earth's mantle: possible sources of primordial isotopes and implications for mantle structure. *Phys. Earth Planet. Inter.* **148**, 13–38.
- Trieloff M., Kunz J., Clague D. A., Harrison D. and Allegre C. J. (2000) The nature of pristine noble gases in mantle plumes. *Science* **288**, 1036–1038.
- Turner S. and Hawkesworth C. (1998) Using geochemistry to map mantle flow beneath the Lau Basin. *Geology* **26**, 1019–1022.
- Vallier T. L., Jenner G. A., Frey F. A., Gill J. B., Davis A. S., Volpe A. M., Hawkins J. W., Morris J. D., Cawood P. A., Morton J. L., Scholl D. W., Rautenschlein M., White W., Williams R. W., Stevenson A. J. and White L. D. (1991) Subalkaline andesite from the Valu Fa Ridge, a back-arc spreading centre in the Lau basin: petrogenesis, comparative chemistry and tectonic implications. *Chem. Geol.* **91**, 227–256.

- Viereck L. G., Flower M. F. J., Hertogen J., Schmincke H. U. and Jenner G. A. (1989) The genesis and significance of N-MORB sub-types. *Contrib. Mineral. Petrol.* **102**, 112–126.
- Wallace P. J. and Carmichael I. S. E. (1992) Sulfur in basaltic magmas. *Geochim. Cosmochim. Acta* **56**, 1863–1874.
- Wallace P. J. (2005) Volatiles in subduction zone magmas: concentrations and fluxes based on melt inclusion and volcanic gas data. *J. Volcanol. Geotherm. Res.* **140**, 217–240.
- Watson E. B. (1991) Diffusion of dissolved CO₂ and Cl in hydrous silicic to intermediate magmas. *Geochim. Cosmochim. Acta* **55**, 1897–1902.
- Webster J. D. (1990) Partitioning of F between H₂O and CO₂ fluids and topaz rhyolite melt – implications for mineralizing magmatic–hydrothermal fluids in F-rich granitic systems. *Contrib. Mineral. Petrol.* **104**, 424–438.
- Woodhall D. (1985) Geology of the Lau Ridge. In *Geology and Offshore Resources of Pacific Island Arcs – Tonga Region* (eds. D. Scholl and T. Vallier). Circum-Pacific Council for Energy and Mineral Resources, Houston, TX, pp. 351–378.
- Workman R. K., Hart S. R., Jackson M., Regelous M., Farley K. A., Blusztajn J., Kurz M. and Staudigel H. (2004) Recycled metasomatized lithosphere as the origin of the enriched mantle II (EM2) end-member: evidence from the Samoan volcanic chain. *Geochem. Geophys. Geosyst.* **5**. ARTNQ04008.
- Workman R. K., Hauri E., Hart S. R., Wang J. and Blusztajn J. (2006) Volatile and trace elements in basaltic glasses from Samoa: implications for water distribution in the mantle. *Earth Planet. Sci. Lett.* **241**, 932–951.
- Yatsevich I. and Honda M. (1997) Production of nucleogenic neon in the Earth from natural radioactive decay. *J. Geophys. Res.: Sol. Earth* **102**, 10291–10298.
- Yamamoto J., Nishimura K., Sugimoto T., Takemura K., Takahata N. and Sano Y. (2009) Diffusive fractionation of noble gases in mantle with magma channels: origin of low He/Ar in mantle-derived rocks. *Earth Planet. Sci. Lett.* **280**, 167–174.
- Zellmer K. E. and Taylor B. (2001) A three-plate kinematic model for Lau Basin opening. *Geochem. Geophys. Geosyst.* **2**, 2000GC000106.

Associate editor: Pete Burnard